The Development of an In-situ Mud Floc Microscope Imaging Device and In-situ Floc Observations from the Lowermost Mississippi River

Ryan T. Osborn

Thesis submitted to the Faculty of the

Virginia Polytechnic Institute and State University

in partial fulfillment of the requirements for the degree of

Master of Science

in

Civil Engineering

Kyle B. Strom, Chair

Nina Stark

Jonathan A. Czuba

May 12, 2021

Blacksburg, Virginia

Keywords: Flocculation, Instrumentation, Machine Learning, In-situ Floc Observation, Cohesive Sediment, Rouse Profile, Floc Settling Velocity

The Development of an In-situ Mud Floc Microscope Imaging Device and In-situ Floc Observations from the Lowermost Mississippi River

Ryan T. Osborn

(ABSTRACT)

Mud makes up a large fraction of sediment transported within rivers to the coasts. Predicting where mud will settle is complicated by the cohesive nature of silts and clays, which can combine to form larger aggregates known as flocs. The size and density, and consequently, the settling velocity, of flocs is highly dynamic and depends on factors such as turbulence levels within the flow and biogeochemical components of the water and sediment. To better predict where mud will deposit, more observations of flocs while in their natural environment is required to better understand the controls on when, where, and to what degree mud is flocculated. However, the need for more field observations is complicated by the dynamic and fragile nature of flocs. This necessitates the need for developing in-situ observation methods to ensure that measured floc sizes are representative of their in-situ size, and not a result of sampling methods. In this thesis, a new instrument for in-situ observation of flocs is presented. In addition, two methods using the data collected from the instrument allow the user to: (1) identify sand within the particle data using a machine learning algorithm, and (2) estimate the mass suspended sediment concentration of the mud and sand fractions of suspended sediment independently. Results from using the instrument in the lowermost Mississippi River reveal differences in floc sizes over the water column, and by season. In addition, a unique observation of flocs in the presence of a salt wedge is presented. Overall, the instrument provided the first known observations of flocs within the Mississippi River, and provides a start to better understanding controls on floc sizes within the fluvial environment.

The Development of an In-situ Mud Floc Microscope Imaging Device and In-situ Floc Observations from the Lowermost Mississippi River

Ryan T. Osborn

(GENERAL AUDIENCE ABSTRACT)

Flowing water within large rivers carries sediments such as sand and mud to the coasts. Some of the larger sediment carried by rivers can fall to the riverbed if the river does not have enough energy to carry it in the flow. The remaining sediment can be carried to the coasts where it will fall to the bed, providing the material necessary for estuaries or deltas to form and grow. Understanding when and where sediment falls to the bed within rivers, estuaries, and deltas, allows scientists and engineers to predict how these landforms will change over time to better manage them under future climate conditions. Predicting where mud will fall to the bed is particularly difficult because mud has the ability to stick together to form larger aggregates. These aggregates, known as mud flocs, are constantly changing in size depending on the energy in the river and water conditions. As the mud flocs change in size, the speed at which they fall to the bed changes. As such, observing mud flocs while they are in their natural environment is required to understand the conditions under which they form and change in size. This thesis presents a new instrument that can be used to collect images of mud flocs while they are in their natural environment. Results from using the instrument to observe mud flocs in the lowermost Mississippi River are then presented. This new instrument, and observations of mud flocs made with it, provides new insight into mud floc size within the lowermost Mississippi River.

Acknowledgments

I would like to express my deepest appreciation to my advisor, Dr. Kyle Strom, for the opportunity to pursue my master's studies and research at Virginia Tech. Your knowledge, guidance, and support have been instrumental to my success and has been appreciated immensely.

To the current and past members of the Baker Environmental Hydraulics Laboratory, thank you for making the lab the playground that it is for exploring hydraulics and sediment. Thank you, Brandon, for letting me borrow your tools and always being ready to provide an off the cuff whiteboard lesson. Thank you, Ehsan, for listening and providing critical feedback on my work, and for being a good friend. Tom, thank you for your help in making data collection run smoothly during Mississippi River surveys, and for the great cooking.

I would like to thank Jeff Nittrouer and Kieran Dunne for sharing their knowledge, suggestions, and feedback on this work. Thank you both for the fun and memorable times down on the Mississippi. I would like to extend my sincerest gratitude to Dr. Nina Stark and Dr. Jonathan Czuba for dedicating your time to serve on my committee. I am extremely thankful to the Via endowment and the New Horizons Graduate Scholars for their financial support. In addition, I would like to thank Renee Cloyd for the support and effort that she puts into the New Horizons Graduate Scholars program to ensure students are progressing through their studies. Finally, last but far from least, thank you to my family and friends for your love and support throughout my academic endeavors. To my parents, Kevin and Gloria Osborn, thank you for always encouraging me to pursue my interests. Your encouragement has played a significant role in shaping who I am today.

Contents

List of Figures

List of Tables

List of Symbols and Abbreviations

α	Stratification adjustment factor
κ	von Karman's constant
ν	Fluid kinematic viscosity
ρ	Water density
ρ_0	Primary particle density
ρ_a	Particle apparent density
ρ_s	Sediment density
τ_*	Dimensionless bed shear stress
τ_{*s}	Skin friction component of bed shear stress
$\forbidden{V}_f$	Floc volume
$\forbidden{V}_{IM}$	Image sample volume
A	Particle area
b	Reference elevation above the bed
C	Suspended sediment concentration
C_b	Near-bed suspended sediment concentration
C_{5t}	Suspended sediment concentration at 5% of the flow depth from the bed

d	Particle diameter
d_f	Floc equivalent circular diameter
d_p	Primary particle diameter
$d_{\#}$	Particle diameter where #% is finer by volume
Fr	Froude number
G	Turbulent shear rate
g	Acceleration of gravity
H	Flow depth
l	Particle resolution factor
N_{f2}	Floc 2D fractal dimension
N_{f3}	Floc 3D fractal dimension
p	Particle perimeter
R_s	Particle submerged specific gravity
S_0	Water surface slope
U	Depth averaged flow velocity
u_*	Shear velocity
u_{*s}	Skin friction component of shear velocity
W	Maximum sample width
w	Variable sample width

w_s Particle settling velocity

z Elevation above the bed

Z_R Rouse number

Chapter 1

Introduction

1.1 Background and motivation

Around 10% of the world's population lives in coastal areas that are below 10 meters above sea level (McGranahan et al., 2007). As sea levels are predicted to continue to rise, these coastal communities will be more susceptible to displacement as the sea encroaches along the coast and increases the likelihood of flooding (Day et al., 2008). Coastal Louisiana is one such area that is currently experiencing a significant amount of land loss due to sea level rise, subsidence, and a cutoff of sediment supply as a result of levees built for flood protection (Morton, 2003; González and Tornqvist, 2006; Colten, 2018). In addition, with the prediction of increases in frequency and intensity of storms, higher land loss rates could be expected if the ecosystem is not allowed enough time to recover between storm events (Emanuel, 2005). One component of the observed land loss along coastal Louisiana is a lack of a sufficient sediment supplied to the existing wetlands to counteract erosion and subsidence. However, the nearby Mississippi River carries a large amount of sediment that is contained within the levee-lined channel. Sediment carried by the river could be passed through targeted sediment diversion with the purpose of contributing to land building along coastal Louisiana (Kim et al., 2009; Kenney et al., 2013). Though, the planning of sediment diversions will require the ability to model and predict the fate of diverted sediment.

Sediment within the Mississippi River consists of both sand and mud (silt and clay particles smaller than 63 μm). While the sand fraction of sediment is relatively easy to model,

modeling the mud fraction is complicated by the cohesive nature of mud that allows for aggregation of the individual silt and clay particles into larger units known as flocs (Fig. 1.1b). When modeling the transport of sediment, the parameter required for accurate modeling is the sediment particle settling velocity. The relatively uniform density and shape of sand allows for accurate modeling of the settling velocity of the sand fraction of sediment. However, for flocs, floc size, shape, and compactness depends on many environmental parameters such as turbulent shear rates, water ion and biological content and makeup, as well as the mineral composition of the silt and clay particles (Eisma, 1986; Mietta et al., 2009). As a result, floc density, and consequently, floc settling velocity, varies as these parameters change. Therefore, modeling of mud requires the knowledge of when, where, and to what degree mud is flocculated within the natural environment. Because these characteristics of flocs are linked to the water conditions under which they form, separating them from their environment has the potential of changing their size and shape due to of the sampling method used. This fragile nature of flocs necessitates the need to develop new methods for in-situ observation to obtain accurate size information of flocs within their natural environment.

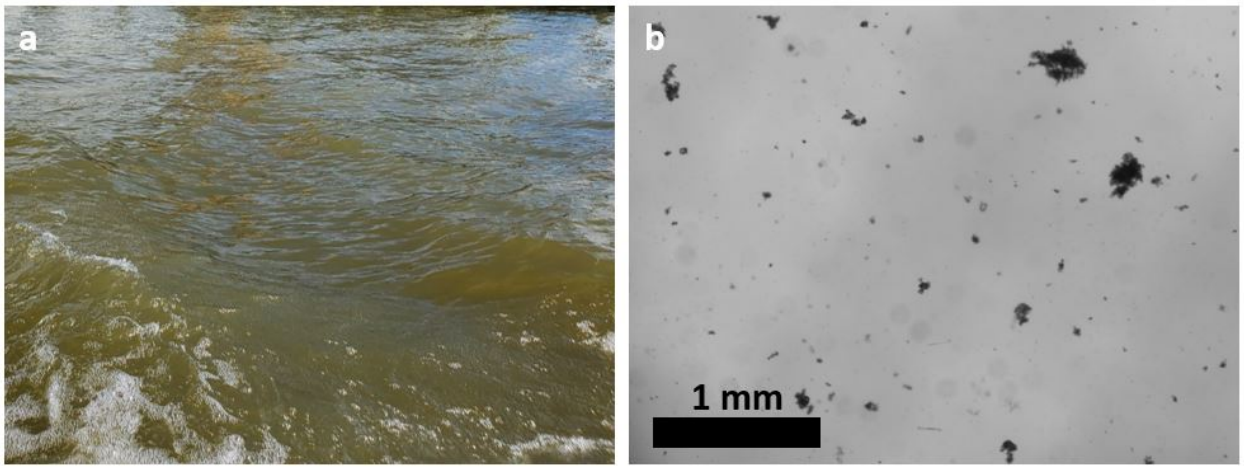

Figure 1.1: (a) Image of the Mississippi River taken while on board the research boat. (b) Zoomed in picture of flocculated mud imaged within the Mississippi River.

Studying flocs within the lowermost Mississippi River provides three unique zones to

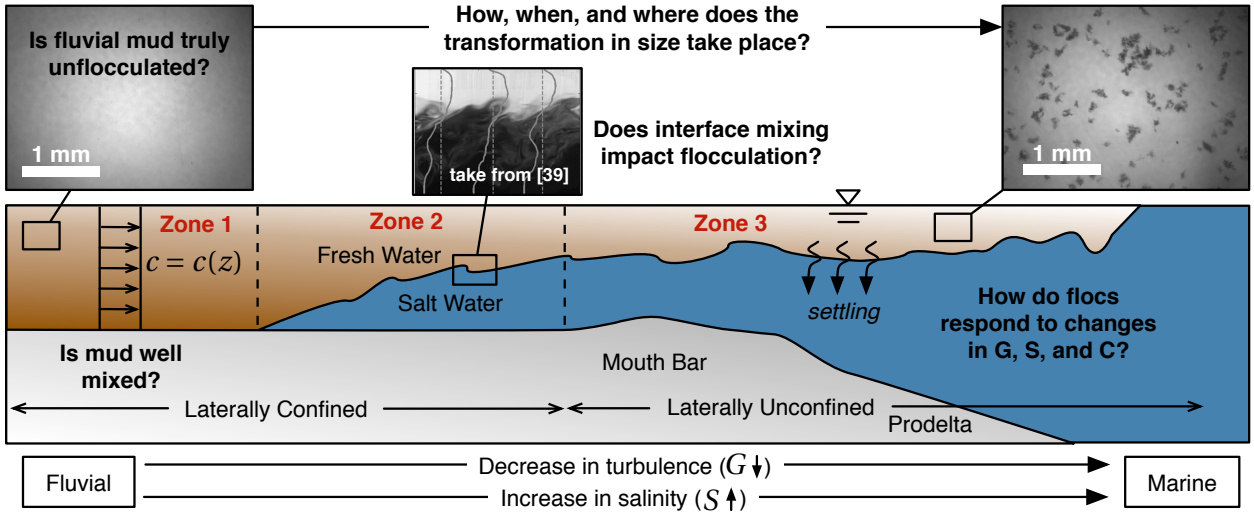

Figure 1.2: Sketch of the fluvial to marine transition for a microtidal distributary channel, where G represents turbulent shear rate, S represents salinity, and c represents suspended mud concentration.

observe floc evolution (Fig. 1.2). These zones include: Zone 1 - the laterally confined, high energy, freshwater zone of the Mississippi River; Zone 2 - the laterally confined zone where freshwater and saltwater meet and mix; and Zone 3 the laterally unconfined zone in the sediment plume within the Gulf of Mexico. These three zones provide unique environmental drivers that shape floc characteristics.

1.2 Goals, hypotheses, and thesis organization

The two broad **research goals** of my thesis work were to:

1. develop an instrument that allows for in-situ observation and measurement of flocculated sediment within freshwater and marine environments; and

2. to make vertical profile measurements of floc sizes in the lowermost Mississippi River that would allow for testing of specific hypotheses associated with the flocculation behavior and implications of mud in the system.

Chapter 2 of this thesis focuses on the camera system developed to meet research goal 1. Chapter 2 has been submitted for review as a stand-alone manuscript to the *Journal of Geophysical Research: Earth Surface*.

The floc camera system developed and described in Chapter 2 was also used to observe flocs within zones 1-3 of the lowermost Mississippi River. In this thesis, I focus on analyzing data from Zones 1 and 2 only. Flocs in Zone 1 are observed within the Mississippi River near the Bonnet Carré Spillway and the Mississippi River near Venice, LA; both of which are upriver from the major distributaries within the delta. Zone 2 measurements were taken along Southwest Pass in the presence of a salt wedge. Two of the **specific hypotheses** that the collected data are used to test are: (H1) that mud is flocculated in the freshwater reaches of the river and contributes to vertical stratification of mud concentration; and (H2) that floc sizes undergo growth in size in the mixing layer of a marine salt wedge. The work associated with research goal 2 is presented in Chapter 3 of this thesis as a stand-alone draft manuscript.

Taken together, the development of the camera system and the in-situ observations of flocs in the field work to inform both modeling efforts as well as experimental efforts focused on understanding and predicting how floc size and settling velocity changes between these two zones.

1.3 Attribution of work in Chapters 2 and 3

For Chapter 2: Ryan Osborn contributed to study conception and design, data acquisition, analysis and interpretation of data, writing of manuscript. Brandon Dillon contributed to study conception and design, and revisions of manuscript. Ehsan Abolfazli contributed to data acquisition, analysis of data, and revisions of manuscript. Kyle Strom contributed to study concept and design, analysis of data, and revisions of manuscript. Kieran Dunne and

Jeffrey Nittrouer contributed to acquisition of data.

For Chapter 3: Ryan Osborn contributed to study conception and design, data acquisition, analysis and interpretation of results, and writing of manuscript. Kieran Dunne contributed to acquisition and analysis of data associated with the P-63 water samples, Shipek grab samples, and ADCP. Kyle Strom contributed to study conception and design, acquisition of data, interpretation of data, and revisions to manuscript. Jeffrey Nittrouer contributed to study conception and design, and acquisition of data. Ehsan Abolfazli contributed to acquisition of data.

Chapter 2

FlocARAZI: An in-situ image-based particle sizing instrument capable of estimating SSC and distinguishing sand from flocs

Ryan Osborn[1], Brandon Dillon[1], Duc Tran[2], Ehsan Abolfazli[1], Kieran B.J. Dunne[3], Jeffrey A. Nittrouer[3], and Kyle Strom[1]

[1]Civil and Environmental Engineering, Virginia Tech, Blacksburg VA USA

[2]IFREMER, DYNECO/DHYSED, ZI pointe du Diable, CS10070 Plouzané, France

[3]Rice University, Department of Earth, Environmental, and Planetary Sciences, Houston, TX, USA

Submitted for review to the *Journal of Geophysical Research: Earth Surface* in April 2021.

2.1 Abstract

An inexpensive and compact underwater digital camera imaging system was developed to collect high resolution images of flocculated suspended sediment at depths of up to 60 meters. The camera has a field of view of 3.7 x 2.8 mm and can resolve particles down to 6 μm. Depending on the degree of flocculation, the system is capable of accurately sizing particles to concentrations up to 500 mg/L. By utilizing the 2D floc geometry and treating the imaged flocs as fractal aggregates, a method is introduced for estimating the mass suspended sediment concentration (SSC) for a series of images. Using the output of the image processing routine, an additional processing step is introduced for identifying sand grains within the particle data, thereby allowing for the separate sizing of sand and flocculated mud in the same set of images.

2.2 Plain language summary

Rivers carry large quantities of muddy sediment that finds its way into river beds, floodplains, lakes, reservoirs, and coastal water bodies. Scientist and engineers rely on measurements of sediment size to understand how sediment moves in a river and where it ultimately deposits. Yet, measurement of muddy sediments (sediment made up of particles with a diameter less than 63 microns) has proven difficult to accomplish. The reason for this has to do with the small size of the sediment and the ability of the smaller particles to stick together to form aggregates that change their size by growing or shrinking depending on the conditions in the flow. This means that accurate measurement of their size cannot be achieved by taking water samples to a laboratory for analysis. In this paper, we present an imaging system we developed to allow for measurement of these sediment aggregates, or flocs, in the water column. The system is relatively inexpensive, reproducible, and is capable of providing

higher spatial and temporal resolution of the suspended particle sizes than any other imaging system previously developed. In the paper we describe the system, test and validate it in the laboratory and field, and show how the data can be processed to provide unique information about the type and amount of sediment available in the water column.

2.3 Introduction

2.3.1 Overview

Mud (sediment mixtures of grain size less than 63 μm) can constitute a significant fraction of sediment transported by rivers to deltaic zones. For this reason, the fate of mud has many implications for the health of deltaic systems, maintenance of navigation channels, and future planning of coastal restoration projects. Consequently, the ability to accurately model the transport and fate of mud is necessary for understanding the historic and future trajectory of many coastal systems. The sediment property most importance for accurate modeling of mud transport is the settling velocity. While estimating settling velocities for particles such as sand is relatively straight forward, estimating the settling velocity of mud is complicated by the ability of constituent mud particles to aggregate into flocs under the right hydrodynamic and biogeochemical conditions (Mietta et al., 2009; Eisma, 1986). Therefore, understanding when, where, and to what degree mud is flocculated is vital to informing sediment transport models. A range of methods have been employed to characterize flocs both in and extracted from their natural environment. Such methods include in-situ and ex-situ settling columns combined with imaging systems to measure floc size and settling velocity, in-situ imaging devices for measuring floc size, and laser-based methods for measuring particle size and volume concentration such as the Sequoia Scientific Laser In-situ Scattering and Transmissometry (LISST) 100x and 200x. In this paper we introduce a new low-cost,

in-situ profiling floc imaging and image-processing system capable of providing separate size populations of suspended mud (both flocs and solid particles) and sand in the size range of 5 to 600 μm (in the current configuration) at a higher resolution and frequency than has been accomplished in the past.

2.3.2 Background

A method that has been used to characterize mud flocs, or the potential of mud to flocculate, is that of settling column tests. Traditional settling tests consist of placing a suspension within a graduated cylinder and observing the rate at which different classes of particles within the suspension settle (Galler and Allison, 2008). With this method, the rate of settling observed for the different classes can be related to grain size through a settling velocity relationship such as Stokes' law. The grain size range observed from the settling tests can then be compared to disaggregated grain sizes to estimate the degree of flocculation present in the suspension. While such a method is simple to execute and an estimate of floc sizes can be calculated, the full range of in-situ floc size and settling velocity is not captured when the sediment is separated from the turbulent river environment and floc size is not observed directly (Milligan and Hill, 1998). Further, extracting a sample for settling column experiments on-shore or on-board a vessel involves multiple steps with possible disruption to flocs and uncertainty that measurements reflect in-situ floc properties.

In-situ settling column and particle sizing systems aim to minimize the disruption to flocs and provide information on their size and density, which is closely tied to the environmental conditions in which they exist. The addition of imaging sediment within the settling column provides the means for a direct measurement of floc sizes and settling velocity through particle tracking. Examples of settling column imaging systems include the IN Situ SEttling Velocity instrument (INSSEV) (Fennessy et al., 1994), Remote In-situ Particle

Settling Camera (RIPScam) (Cartwright et al., 2011), and the Particle Imaging Camera System (PICS) (Smith and Friedrichs, 2011). Images from the INSSEV system capture settling velocity directly by tracking particle motion frame-by-frame. This method requires that disturbances to the system be minimized to reduce external influence on the particles settling within the settling column. Stability with the INSSEV system is maintained by locating the system on a weighted tripod that is positioned on the bed during sampling (Manning and Dyer, 2002). Consequently, the system is limited to measuring particle size and settling velocity at the level of the tripod. Both the RIPScam and PICS are capable of estimating settling velocity and particle size over the full range of the water column. These systems can be lowered to a desired depth, where a water sample is collected within the settling column and separated from the external flow by closing both ends of the settling column. Images are then collected after the settling column is closed on both ends. Estimating floc settling velocity with these systems is achieved by employing particle tracking velocimetry (PTV) to measure the velocity of individual flocs, and particle image velocimetry (PIV) to estimate the background fluid velocity by tracking particles smaller than 2 pixels (Smith and Friedrichs, 2015). For a series of images, the settling velocity for a floc is estimated as the vertical component of the average vector subtraction of the fluid velocity from the floc velocity. Of the aforementioned imagine systems, the RIPScam has a similar resolution as the other systems (down to 20 μm), but the widest observable particle size range (up to 20 millimeters). The resolution of the INSSEV and PICS is approximately 20 to 900 μm and 30 to 1000 μm, respectively. These systems were designed for and perform well for the purpose of measuring floc size and settling velocity at targeted locations. However, the nature of settling velocity measurements requires longer periods of time to collect measurements at a particular field location compared to collecting particle size information alone, as can be done with a device such as a LISST-100x. Further, settling column systems are limited to collecting discrete samples separated from the flow, as opposed to continuous sampling over

the water column.

In-situ particle sizing by means of laser diffraction was first introduced by Bale and Morris (1987). The instrument was developed by transferring the components of a Malvern Model 2200 particle sizer to a field-deployable waterproof housing. Depending on the focal length of the receiving lens, the instrument could resolve particles in the range of 1.2 to 5.8 μm and up to 564 μm. Laser diffraction instruments rely on Mie's theory to relate the angle and intensity of light scattering to particle size (Mie, 1908). Two of the most widely known laser diffraction in-situ particle sizing instruments include the LISST 100x and 200x manufactured by Sequoia Scientific (Agrawal and Pottsmith, 2000). The output from measurements taken with the LISST instruments is a volume-based distribution with 32 logarithmically spaced bins in the range of 2.5-500 μm for the LISST 100x and 36 bins in the range of 1-500 μm for the LISST 200x. Both of these instruments rely on logarithmically spaced detector rings to capture laser light scattered by particles passing through the measured control volume. A major advantage of the LISST instruments is their ability to measure particles without significant disruption to the particles or flow. Further, the compact size of the instrument allows for easy handling and data collection when profiling over the water column from a small research vessel. However, caution has been advised when using the LISST instruments when concentration of small particles (< 58 μm) is of interest (Graham et al., 2012; Filippa et al., 2011) and when particles larger than the 500 μm upper limit of detection are preset, which can lead to an overestimate of particles within the larger size bins (Davies et al., 2012). Questions still remain as to how laser diffraction particle sizers perform when dealing with particles of complex shape and variable density (Graham et al., 2012; Karp-Boss et al., 2007; Felix et al., 2013). Additionally, in areas of large density gradients such as pycnoclines, both a Digital Floc Camera (DFC) (Mikkelsen et al., 2008) and a LISST-100x were observed to falsely measure increases in particle size and concentration due to the schlieren effect (Karageorgis et al., 2015). However, while data collected with the LISST-100x cannot be

processed to exclude artifacts from the schlieren effect, the images collected with the DFC were processed to exclude regions within the images where the schlieren effect was present. Due to the possibility of inaccuracy with LISST devices under certain circumstances, LISST instruments have been deployed in conjunction with image-based devices both to extend the observable range of particle sizes and to provide verification that both devices are sizing particles accurately (Fall et al., 2021; Mikkelsen et al., 2006; Davies and Nepstad, 2017; Mikkelsen et al., 2005).

In addition to in-situ settling columns with imaging systems and laser diffraction particle sizing instruments, in-situ imaging systems for imaging sediment continuously over the water column have been developed. These systems have been developed both to extend the range of other particle sizing instruments, for example, combining a LISST-100x with a DFC (Mikkelsen et al., 2006; Hill et al., 2011), and as a verification of the output from instruments such as the LISST-100x (Mikkelsen et al., 2005). The DFC can measure particles in the range of 135 – 9900 μm, producing a combined range of 2.5 – 9900 μm when combined with the LISST-100x particle size distribution. Others have constructed camera imaging systems as a lower cost alternative to retail products (Benson and French, 2007). The In situ Particle Imaging Device (InSiPID), developed by Benson and French (2007), combines two cameras with differing magnification to produce a measurable range of 4 - 3000 μm.

Image-based particle sizing instruments suffer from two main problems, namely, an adequate light source that is capable of producing enough light to illuminate particles at high shutter speeds to minimize particle streaking, and long periods of time needed for image processing. In the past, the problem of adequate lighting has been resolved by using a strobe light source matched with image acquisition by means of a programmed micro-controller (Benson and French, 2007; MacDonald and Mullarney, 2015). Though image processing routines still require a significant amount of time to identify and size particles compared to devices such as the LISST-100x, these routines can be automated, requiring little

user intervention during processing (Keyvani and Strom, 2013; Smith and Friedrichs, 2015). Compared to laser diffraction methods, in-situ imaging systems have the benefit of providing users with the ability to visually observe and characterize the particles that are eventually sized. This allows users to better understand influences on and explain possible discrepancies between particles size information obtained from different instrument (Mikkelsen et al., 2005; Davies et al., 2012; Mikkelsen et al., 2008).

2.3.3 Purpose

In this paper we introduce a new, low cost and compact suspended sediment imaging system called the FlocARAZI (Floc AReA and siZing Instrument). The FlocARAZI is designed to image flocculated sediment that is allowed to pass freely through a flow-through cell, minimizing interaction of sediment with the device and allowing for continuous profiling of suspended sediment over the water column. The cost of the system is reduced by using off-the-shelf and 3D printed parts. Power and signal to the camera, and a continuously illuminated light source, are controlled at the surface through two ethernet cables, allowing for real-time monitoring of the camera feed during deployment. The design of the system is simple to allow for ease of reproduction by others. In addition to introducing the camera in this paper, we also present two methods that use the output of a previously developed image processing routine to provide unique information about the suspension. First, a method is introduced to estimate the mass suspended sediment concentration (SSC) of flocculated sediment from the collected image data. The ability to estimate SSC from FlocARAZI image data provides the means to collect higher resolution SSC information over the water column than could be obtained with physical water samples alone. The second processing method introduced utilizes floc and sand size and texture properties to train a support vector machine (SVM) learning algorithm to classify suspended sediment particles as either sand or

flocculated mud. The ability to distinguish between flocs and sand is a key benefit of in-situ imaging devices, especially when properties of flocs, rather than the full range of particles in suspension are of interest. Once trained, the learning algorithm provides an accurate way to quickly identify sand within the particle data output from the image processing routine.

2.4 FlocARAZI

The FlocARAZI (Fig. 2.1) consists of a camera mounted to a stepper-motor-driven linear slide rail stage, and an LED for illuminating the camera field of view. The camera, stepper motor, and LED are powered and controlled from the surface by two 60-meter-long weatherproof Cat6 ethernet cables. A direct connection to the surface allows for a real-time camera feed and in-situ adjustment of the camera focus and LED brightness. The camera is a monochrome 4000 x 3000 pixel FLIR Blackfly S GigE with a CMOS Sony IMX226 sensor that has a pixel size of 1.85 μm, and is capable of collecting images at a rate of up to 10 frames per second. The camera lens assembly consists of a 5X Mitutoyo plan apochromat, infinity corrected, long working distance objective mounted to a ring-actuated aperture stopped down to f/21.4. The maximum f-number of the system is f/6.3. The objective is positioned at the end of a 78 mm SM1 threaded tube containing an achromatic doublet lens with a focal length of 75 mm. The combination of the 5X Mitutoyo objective with the achromatic doublet lens produces an effective magnification of 2X, resulting in an image pixel size of 0.925 μm and a nominal field of view of 3.7 x 2.8 mm. A stepper-motor-driven 150 mm linear slide rail allows for focusing of the camera during deployment. The LED is a 6 V CREE Mt-G2 Q0 on a Noctigon Mt-G20 MCPCP rated for a maximum nominal light output of 1990 lumens at 18.5 watts.

The camera assembly and LED are housed in separate BlueRobotics 3-inch diameter watertight acrylic tubes that are rated to 150 m depth. A flow-through cell consisting of

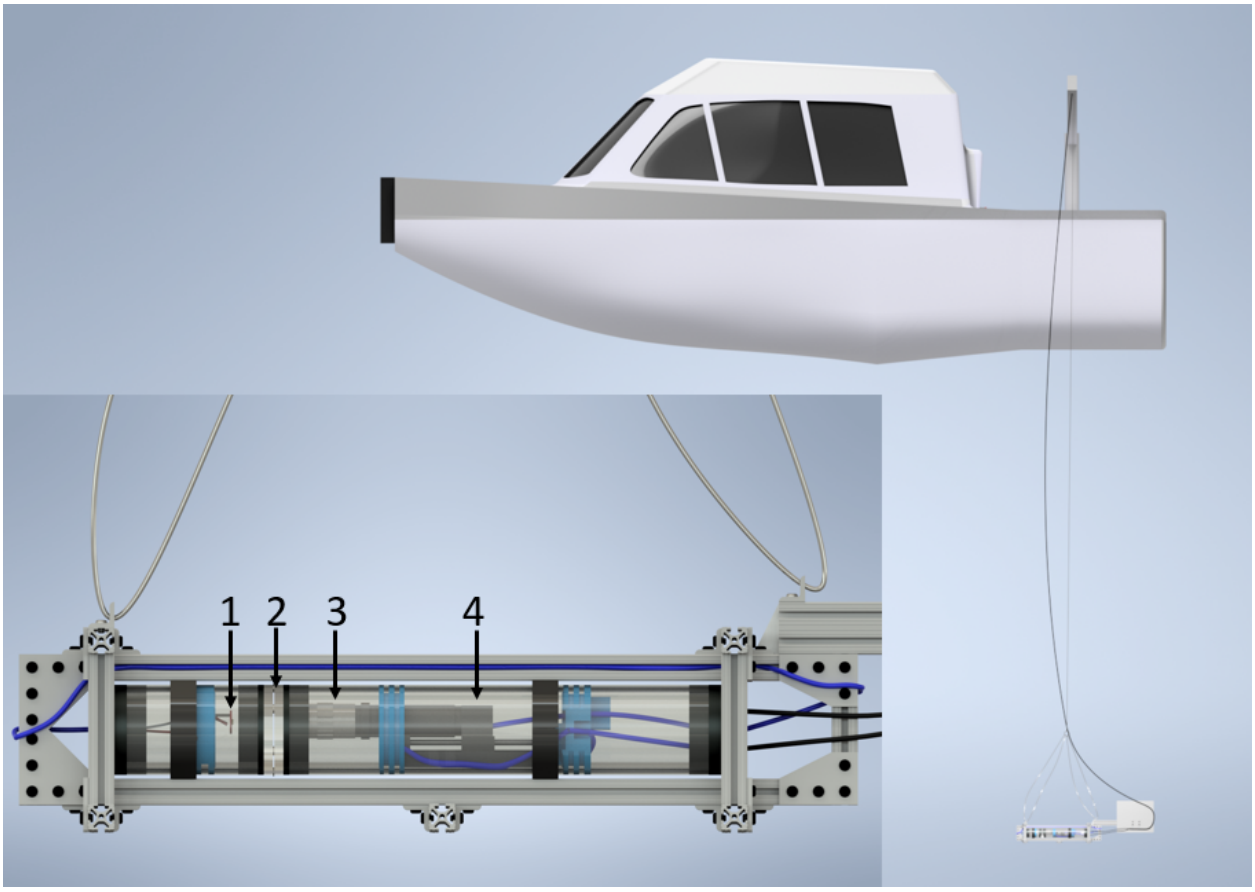

Figure 2.1: The FlocARAZI both in its deployed state and a close up side view identifying the (1) LED, (2) 1.17 mm flow-through cell, (3) Mitutoyo objective and lens assembly, (4) camera. The black wires entering the camera tube control and send a live video feed to the surface.

two acrylic end caps with a 1.17 mm gap, through which water and sediment are free to flow, separates the camera and LED tubes (Fig. 2.1). The acrylic end caps are secured together in concentric alignment with six tapered stainless-steel screws positioned within six equally spaced through holes along the perimeter of the acrylic end caps. The gap width can be adjusted for different applications by placing spacers of the desired thickness between the acrylic end caps before tightening the screws. The camera is set to focus on the center of the flow-through cell gap by means of adjusting the linear slide rail stage position through controlling the stepper motor. One-inch aluminum T-Slotted framing rails are uses to support the acrylic tubes and provide mounting points for a hoist connection and additional equipment. To maintain a consistent orientation into the flow, a 36.5 x 31 cm, 1.5 mm thick aluminum plate is mounted to the framing to act as a rudder.

While the FlocARAZI is deployed, the camera is powered and transmits a live video feed through one of the two 60-meter-long Cat6 ethernet cables, with power supplied by a power over ethernet injector. The video feed is displayed and recorded through the FLIR SpinView GUI. The second ethernet cable supplies a signal to the stepper motor, for controlling the linear slide rail platform position, and power to the LED. Power is supplied to the LED by a DC power supply through four of the 8 available ethernet wires, which allows for adjustment of the brightness by changing the current supplied to the LED. Power to the stepper motor is supplied by an onboard 7.4 V, 1500 mAh battery. The remaining 4 wires in the second ethernet cable send direction and speed controls to the stepper motor for focusing the camera.

2.5 Validation and test deployment

2.5.1 Sizing: image processing and validation

The ability of the camera system and processing routine to resolve and accurately size particles in suspension was tested by conducting controlled laboratory experiments in which PIV seeding particles were imaged. The images were then processed to obtain a size distribution that was compared to a particle size distribution obtained by sizing the seeding particles with a HORIBA LA-300 laser scattering particle-size distribution analyzer. The image processing routine was then updated to best match the camera-produced size distribution with that from the HORIBA LA-300. Due to the relatively large size of the FlocARAZI compared to available testing tanks, the modified setup shown in figure 2.2 had to be used. The setup consists of a 13-liter acrylic mixing tank, and the same LED light source and camera assembly described in the previous section. The spacing of the flow-through cell was maintained by fixing the same 1.17 mm spacers between the LED light source and the wall of the mixing tank, though the actual width was measured to be 1.55 mm due to added thickness from adhesive material.

Images for these experiments and others are processed following the general method of Keyvani and Strom (2013), which employs an automated script that identifies all particles within an image, via an ImageJ (Rasband, 2012) macro, and removes out-of-focus particles within MATLAB R2013B. The ImageJ macro provides individual particle information such as area, perimeter, fit ellipse dimensions, shape descriptors, bounding box dimensions, and particle location within the image, for each image. The MATLAB script then uses the previously obtained particle location to obtain the pixel intensity matrix of the bounding box for each particle within the image set, and determines the clarity and contrast of each particle. The clarity of a particle is a measure of the steepness of the pixel grey scale values near the edge of the particle. The contrast is a measure of the difference in pixel intensity

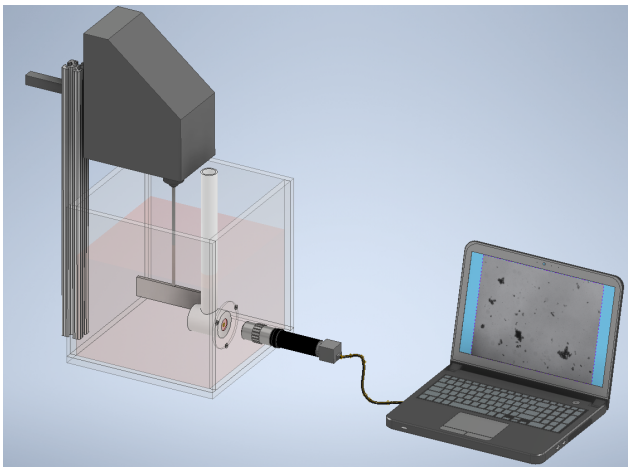

Figure 2.2: Mixing tank setup used for validating FlocARAZI camera. The same 1.17 mm flow-through cell spacers were used in an attempt to mimic the flow-through cell present on the FlocARAZI.

for the pixels that make up the particle. Particles with a clarity value greater than 0.7 were assumed to be in focus and their information was retained. For those particles deemed in focus, the equivalent circular diameter of each floc or solid particle (in pixels), d_f, is calculated within each image from the measured floc area, A, as:

$$d_f = \sqrt{\frac{4A}{\pi}} \tag{2.1}$$

A few minor changes were made to the process of Keyvani and Strom (2013) to account for increased image resolution of the FlocARAZI camera compared to camera used in their study. In the background subtraction step, the rolling ball radius was increased from 50 to 60 pixels and the sliding paraboloid function was included. Additionally, the triangle thresholding function was used instead of the Yen method (Zack et al., 1977). It was determined through trial and error that this combination of rolling ball radius and the sliding paraboloid function with the triangle thresholding was the most robust method for sizing particles in the range of 5 – 600 μm. The last change to the original processing routine was to include a binary erode step after thresholding. The erode function removes one layer of pixels from the edges

of objects within the thresholded image. This step was included so that the outline of the particles identified by ImageJ better matched the expected outline based on the original image.

We determined the lateral resolution of the microscope, as configured, to be 0.925 μm/pixel. This calibration was found by using a stage micrometer slide with ruled divisions of 0.1 mm. On average, 1081.1 pixels were required to image 10 divisions (1 mm) on the reticule.

Validation of the pixel to micrometer conversion and the image processing routine was performed by comparing the camera produced size distribution of 10 and 20 μm PIV seeding particles to the size distribution obtained by a HORIBA LA-300 (Fig. 2.3). The HORIBA LA-300 is a laser scattering particle-size distribution analyzer that is capable of measuring particle in the range of 0.1 to 600 μm. The particles used for the tests were Dantec Dynamics 10 μm Silver Coated Hollow Glass Spheres (S-HGS) and 20 μm Polyamide Seeding Particles (PSP). According to Dantec Dynamics, the S-HGS have a mean particle size of 10 μm and a size distribution of 2-20 μm and the PSP have a mean particle size of 20 μm and a distribution of 5-35 μm. Preparation of each sample for sizing with the FlocARAZI camera consisted of sonicating 30 mg of the seeding particles within a 30 mL vial of tap water. The sample was then added to the 13-liter mixing tank. The paddle speed in the mixing tank was set to a mixing rate of 50 rpms, corresponding to a turbulent shear rate, G, of 90 Hz, which is within the mixing rate range for previous floc studies (Kumar et al., 2010; Mietta et al., 2009; Zhu et al., 2015). The camera collected one image every second for 20 minutes. A size distribution was created (Fig. 2.3) for the 20 minutes of image size data following the aforementioned image processing routine. This process was carried out for both the S-HGS and PSP suspensions. Preparation of the sample for sizing with the HORIBA LA-300 followed a similar procedure, however, the sample was first diluted to a concentration suitable to achieve the light transmission requirements of the system. The

seeding particles in the suspension were measured with the HORIBA LA-300 three separate times and the resulting distributions were averaged to obtain the particle size distributions presented in figure 2.3. The size distribution produced by the FlocARAZI camera and the HORIBA LA-300 are quite similar, with only a slight difference in the mean particle size and standard deviation (Table 2.1).

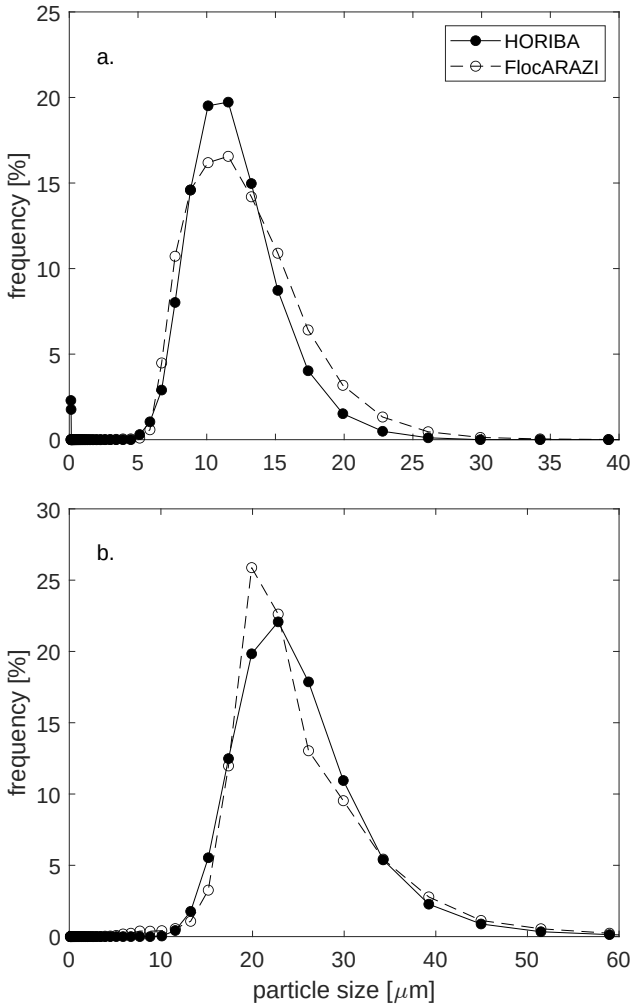

Figure 2.3: Size distribution comparison between (a) 10 μm and (b) 20 μm seeding particles sized with a HORIBA LA-300 and FlocARAZI.

The comparison outlined above shows that, with proper calibration of the conversion from camera pixel length to physical length and the image processing routine, the FlocARAZI

Table 2.1: Particle sizing with HORIBA LA-300 and FlocARAZI camera

Particle Size [μm]	Sizer	Mean [μm]	Std. [μm]
10	HORIBA	10.9	3.7
	FlocARAZI	11.8	3.8
20	HORIBA	23.6	6.3
	FlocARAZI	23.5	7.2

can produced particle size distributions that compare favorably to those of the HORIBA LA-300. Additional testing with the camera in the same lab setting has produced favorable results for flocs in the size range of 50 - 85 μm when compared to older lab cameras that have previously been used and calibrated (Keyvani and Strom, 2013; Tran et al., 2018). The upper limit of the particle size range that the camera system can accurately capture is dependent on the width of the flow-through cell gap and the field of view of the camera. Therefore, the width of the flow-through cell gap should be adjusted depending on the floc size range expected to be imaged. With the current flow-through cell gap and good lighting, the FlocARAZI camera system can accurately size particles in the range of 5 - 600 μm.

2.5.2 Field deployment example

Validation of the FlocARAZI's operation in the field has been tested through deployments of the system within the lowermost sections of the Mississippi River. The FlocARAZI has been successfully deployed to depths of up to 36.5 meters. During these deployments, images collected with the FlocARAZI (Fig. 2.4) have provided floc size information within the main channel of the Mississippi River, its distributaries, and the plume within the Gulf of Mexico at the exit of South and Southwest Pass. Images were collected at a rate of 2 images per second, which by trial and error, was determined to be an adequate rate for allowing sediment to flush through the camera field of view, reducing the likelihood of imaging the

same particles in successive images. Images collected with the FlocARAZI can require a large amount of data storage space. For example, during a 9 day long survey, around 59,000 images were collected with the FlocARAZI, requiring nearly 700 GB of drive storage space. A typical image collected during the survey contained between 50 to 150 in focus particles. Observations with the FlocARAZI revealed d_{50} floc sizes in the range of 70 - 130 μm within the freshwater reaches of the Mississippi River Delta, with the largest flocs observed to be in the range of 400 - 500 μm (Osborn et al., 2020).

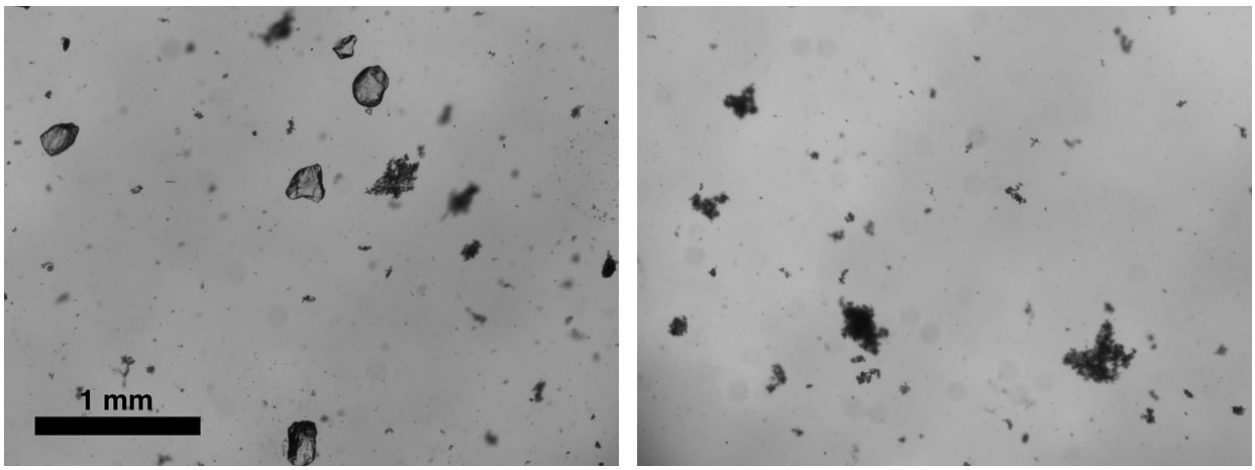

Figure 2.4: Example images collected with the FlocARAZI while deployed in the Mississippi River. Both sand and flocs are present.

2.6 Estimating suspended sediment mass concentration from images

2.6.1 Method overview

The mass concentration of suspended sediment both in the field and laboratory often needs to be measured. In this section we present a method for extracting mass concentration measurements from images collected with the FlocARAZI that can be used to supplement

physical water column samples. Because flocs can be distinguished from sand in these images, the method provides a means of estimating the mass of sand and mud separately under certain assumptions, something that cannot be accomplished with traditional laser or optical methods.

To measure SSC one must know both the dry mass of the sediment within a suspension sample (or the dry volume and sediment density) and the total volume of the sample. To obtain SSC measures from images we estimate the volume of sediment imaged per volume of suspension sampled and then convert the sediment volume to a mass using a specified sediment density. For example, the average mass concentration, C, from a set of n number of images can be defined as,

$$C = \frac{\sum_{i=1}^{n}\sum_{j=1}^{k} \rho_{a,ij} \forbar{V}_{f,ij}}{n \forbar{V}_{IM}} \tag{2.2}$$

where k is the number of particles in each image, $\forbar{V}_{f,ij}$ is the j-th imaged floc or particle within the i-th image, $\rho_{a,ij}$ is the apparent density of that particular floc or particle, and $\forbar{V}_{IM}$ is the volume of the region imaged by the camera. Therefore, to estimate C, one must know the volume of the individual particle, the density of the particles, and volume of fluid being imaged.

The most straightforward of these three parameters to estimate is the particle or floc volume, $\forbar{V}_f$:

$$\forbar{V}_f = \frac{\pi}{6} d_f^3 \tag{2.3}$$

These volume estimates are made for each identified particle in each image using the projected area of the particle or flocs (Eq. 2.1). While equation 2.3 does not provide a true measure of particle volume due to the 2D nature of the images, it is reasonable to expect it to provide a non-biased estimate since particles are measured in suspension without any

directional preference over thousands of particles.

Density estimates for each particle are more complicated to obtain. In each image, it is possible that identified particles could be a solid mineral (sand or silt particle), a porous to semi-porous mud aggregate or floc, or even organic and biological material such as fine particulate organic matter (FPOM) or plankton. The method presented here for estimating particle density does not account for organic or biological material. Though, if organic and biological material represent a small fraction of imaged particles, their effect on the overall SSC would be expected to be minimal. If solid mineral particles can be identified, then the density of those particles can be set to the density of silica sand ($\rho_a = 2650$ kg/m^3 irrespective of particle size). However, estimating the density of the mud fraction is complicated by the irregular structure of mud flocs. The irregular and porous structure of flocs means that floc density can vary from floc to floc and for any individual floc with size. For example, the overall floc density has been shown to be a non-unique power function of floc size (Dyer and Manning, 1999). Due to the irregular and compounding packing structure of flocs, and the measured power-law behavior of floc density with floc size, floc density is often modeled assuming the flocs are 3D fractal aggregates (Li and Ganczarczyk, 1989; Flesch et al., 1999; Maggi et al., 2007). As such, the apparent floc density, ρ_a (defined as the floc's dry mass divided by its wet volume), depends on the characteristic floc size and the density, size, and arrangement of the constituent primary particles that make up the floc:

$$\rho_a = \rho_0 \left(\frac{d_f}{d_p} \right)^{N_{f3}-3} \tag{2.4}$$

In equation 2.4, ρ_0 is the density of the primary particles that make up the floc, d_f is the equivalent spherical diameter of the floc, d_p is the equivalent spherical diameter of the primary particles (Bowers et al., 2017), and N_{f3} is the 3D fractal dimension of the floc. The 3D fractal dimension is not a quantity that can be measured directly from two-dimensional

(2D) images. Therefore, to obtain N_{f3}, and hence floc density, we used the model developed by Maggi and Winterwerp (2004) for converting from a 2D perimeter-based fractal dimension to a 3D fractal dimension. This model allows for using information of floc perimeter and area, obtained from an image, to estimate floc three dimensional fractal dimensions.

Maggi and Winterwerp (2004) developed their model for 3D fractal dimension based on 2D perimeter-based fractal dimension using data they generated by projecting 3D objects of specific 3D fractal dimension onto 2D coordinate planes. Included in their model is a resolution factor, l, that accounts for the fact that the imaged flocs are composed of individual pixels. A hyperbolic like equation was then fit to the data to produce a semiempirical relation for mapping 2D fractal dimensions to 3D fractal dimensions.

To use the method, the perimeter-based 2D fractal dimension, N_{f2}, is computed as:

$$N_{f2} = 2\frac{\log[p]}{\log[A]} \tag{2.5}$$

where the perimeter, p, and area, A, of the individual flocs are in pixels and pixels^2 as obtained in the image processing output.

Next, the resolution factor, l, defined as the pixel length of one side of a square box surrounding an individual floc, is computed. However, since most flocs are bound by a rectangular box, l is obtained by calculating the side length of a square of the equivalent area of the rectangular box surrounding the floc. That is,

$$l = \sqrt{p_x p_y} \tag{2.6}$$

where p_x and p_y are the length and width in pixels of the bounding rectangular box around an individual floc, both of which are outputs of the processing routine. In creating the mapping function, boundary conditions, $z(l)$ and $k(l)$, are introduced to account for the $N_{f2} = (3, z(l))$ and $N_{f3} = (k(l), 2)$ boundaries, respectively. The boundary condition, $z(l)$,

is defined as the 2D fractal dimension of the projection of a box that has a resolution of l:

$$z(l) = \frac{\log[4l-4]}{\log[l]} \tag{2.7}$$

$k(l)$ is defined simply as a function of $z(l)$ by fitting data points at the boundary $N_{f2} = 2$:

$$k(l) = k(z(l)) = z(l)[z(l)-1] + 1 \tag{2.8}$$

A function of the form,

$$N_{f2} = \frac{a}{N_{f3}^2} + b \tag{2.9}$$

was then solved, resulting in the coefficients a,

$$a(l) = 9\left(z(l) - \frac{2[k(l)]^2 - 9z(l)}{[k(l)]^2 - 9}\right) \tag{2.10}$$

and b,

$$b(l) = \frac{2[k(l)]^2 - 9z(l)}{[k(l)]^2 - 9} \tag{2.11}$$

where N_{f3} is the 3D fractal dimension. The 3D fractal dimension of an individual floc can then be estimated by:

$$N_{f3} = \sqrt{\frac{a(l)}{N_{f2} - b(l)}} \quad \text{for} \quad N_{f2} < 2 \tag{2.12}$$

Once N_{f3} is calculated for each floc, using equations 2.5-2.12, the density of each floc, needed in equation 2.2, can be calculated from equation 2.4.

The last measure needed for the estimate of C from equation 2.2 is the imaged volume, $\forall_{IM}$. A simple estimate of $\forall_{IM}$ can be obtained by multiplying the field of view by the

sampling gap size or width created by the acrylic end caps of the camera and light housing (Fig. 2.1). However, the gap size between the acrylic end caps is larger than the camera's depth of field. This means that the volume associated with in-focus particles would be equal to or less than the physical gap size. Furthermore, the perceived imaged volume could be a function of imaged particle size. For example, larger particles could be more likely to be in focus within the depth of field of the camera compared to smaller particles that have a narrower margin to be in focus. To account for this phenomena, we developed a variable width for the imaged volume that is dependent on particle size. The variable width accounts for the smaller particles that are assumed to be within the imaged volume, but not in focus within the image. For our purposes, we took the variable sampling width, w, to be described by a logistic function where the width increases with particle size within a defined range, then asymptotically reaches a constant width:

$$w(d_f) = \frac{W}{1 + e^{-k(d_f - d_0)}} \tag{2.13}$$

The constant width, W, should be taken to be the smaller of the either the width of the gap or the depth of field of the camera, as either of these widths could limit the volume observable by the camera. The logistic growth rate, k, and the sigmoid's midpoint, d_0, are experimentally determined values that are dependent on the depth of field of the particular camera and optics setup.

2.6.2 Experiments to test and calibrate the method

We ran a series of laboratory mixing tank experiments over a range of known SSC values and turbulent mixing rates to calibrate and test the methodology outlined above for estimating C from images.

The experiments were conducted in the same aforementioned 13-liter mixing tank (e.g.,

Tran et al., 2018) (Fig. 2.2). For each run, a known mass of sonicated kaolinite clay was added to the mixing tank to obtain a known SSC. The concentrations tested include 20, 100, 200, 300, 400 and 500 mg/L. An additional 5 mL of a 300 mg/L xanthan gum solution was added to the mixing tank to encourage flocculation. The experiments were conducted at two different turbulent shear rates of approximately 50 and 90 Hz. Before images were collected for the experiment, the flocs formed from the sonicated sediment were allowed to mix for three hours to ensure that an equilibrium size distribution had been reached. After three hours, the camera was set to record one image per second for 15 minutes. The same procedure was then repeated for the remaining mass concentrations and turbulent shear mixing rates. An optical backscatter sensor (OBS) was also placed within the tank to check for settling, though, no settling was observed for any of the test cases.

Images from the experiments were processed to provide floc size information for each floc identified within the set of collected images. This size information was then used in conjunction with the model developed by Maggi and Winterwerp (2004) to estimate a 3D fractal dimension for each floc. Assuming a characteristic primary particle density and size, the apparent density of each floc was estimated using equation 2.4. The mass of each individual floc was then estimated by multiplying the apparent density by its equivalent spherical volume. For the analysis, the primary particle density was set 2500 kg/m^3 and d_p was taken to be 6.6 μm, which is the mean particle size of the kaolinite clay mixture.

A summary of the experimental conditions and resulting floc size statistics at equilibrium is given in Table 2.2

2.6.3 Concentration estimation results

For all test scenarios, SSC was estimated for each minute of the collected image series, both with and without the inclusion of the variable sampling volume width (Eq. 2.13). The SSC

Table 2.2: Average floc sizes for each concentration and mixing rate

SSC [mg/L]	G [Hz]	d_{16} [μm]	d_{50} [μm]	d_{84} [μm]
20	50	15	27	54
20	90	15	34	62
100	50	55	98	141
100	90	30	43	58
200	50	79	109	150
200	90	49	67	93
300	50	100	141	198
300	90	54	77	108
400	50	116	171	245
400	90	64	94	132
500	50	125	195	280
500	90	68	104	151

estimates without the inclusion of the variable width was used to inform the parameters of the variable width logistics equation, namely, the growth rate, k, and the sigmoid's midpoint, d_0. The average of the estimated uncorrected SSC for each scenario is plotted in Figure 2.5a using a constant gap or sample volume width, w, against the known concentration. In all cases except the lowest two concentrations (20 and 100 mg/L), the SSC estimates from the images are greater than the known SSC by a factor of ≈ 4.4. That is, the relationship between C estimated from the images and C known through the addition of a known mass to the mixing tank appears to be linear across the majority of the concentrations.

The variable sampling width, $w(d_f)$ (Eq. 2.13), parameters of k and d_0 were tuned to bring the lower concentration experiments more in line with the linear trend of the higher concentration experiments. The resulting sampling volume width equation that achieves this end is:

$$w(d_f) = \frac{1.55}{1 + e^{-0.2(d_f - 27)}} \tag{2.14}$$

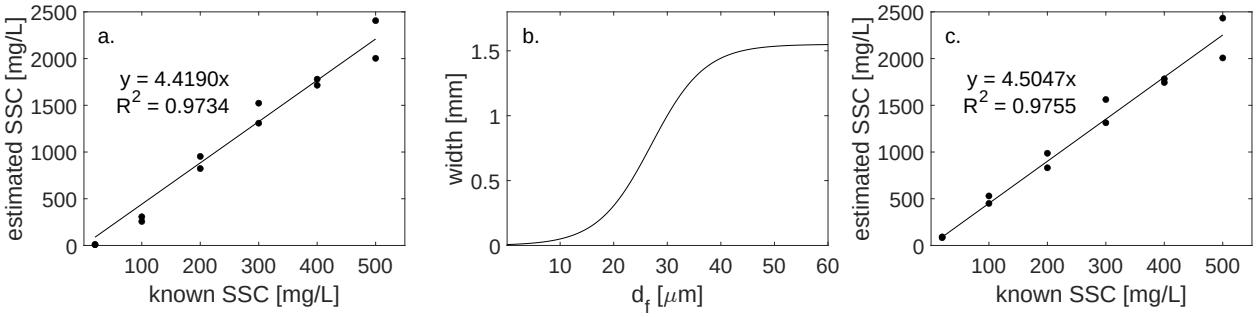

Figure 2.5: (a) SSC estimated using the camera particle data vs. known concentration in the mixing tank. (b) A variable width curve, dependent on floc size, used to account for particles outside of the cameras depth of field. (c) SSC estimated with the inclusion of the variable width curve. The slope of the best fit line, shown here, will be used as an additional correction factor to map the estimated SSC to a corrected SSC.

Equation 2.14 is plotted in Figure 2.5b. The result of defining the sampling volume width using Equation 2.14 on the relationship between estimated SSC from the images and the known SSC is shown in figure 2.5c. The line of best fit, with an intercept passing through the origin, has a slope of 4.5047 and a $R^2 = 0.9755$. It is this fit equation that is used to map originally estimated SSC to corrected SSC. Values of actual, original estimates, and corrected SSC are given in Table 2.3 along with the percent difference between the actual and image-based corrected SSC estimates. The standard deviations for the corrected SSC estimates only deviate slightly from the corrected SSC, revealing that concentration estimates for each minute only deviate slightly from the full 15 minute average.

2.6.4 SSC estimate dependence on d_p

The two user-selected input parameters for the routine used to estimate SSC are the primary particle density, ρ_0, and the primary particle characteristic diameter, d_p. The model's dependence on ρ_0 is linear. Consequently, changing the specified ρ_0 will linearly scale the estimated SSC. However, the estimated SSC is not linearly dependent on d_p (Eq. 2.4). The dependence of the uncorrected estimated SSC on d_p was investigated for all test scenarios

Table 2.3: SSC estimated from image data and linearly scaled corrected SSC estimate

Actual SSC [mg/L]	Mixing rate [Hz]	Estimated SSC [mg/L]	Corrected SSC [mg/L]	Corrected SSC Std. [mg/L]	% diff.
20	50	83.4	18.5	0.8	7.4
20	90	91.6	20.3	0.6	1.7
100	50	450	99.8	2.1	0.2
100	90	530	118	2.0	17.6
200	50	831	184	3.8	7.8
200	90	987	219	2.2	9.6
300	50	1313	291	8.1	2.9
300	90	1562	347	1.9	15.6
400	50	1783	396	7.7	1.0
400	90	1744	387	4.1	3.2
500	50	2007	446	7.7	10.9
500	90	2433	540	3.4	8.0

by observing the shape and magnitude of estimated SSC after setting d_p equal to 2.6 and 10.6 μm (Fig. 2.6). The general behavior of the model to a change in d_p is a decrease in the magnitude of estimated SSC with a decrease in d_p, and an increase with increasing d_p. The linearity of the estimated SSC appears to hold for both choices of d_p. The slope of the line of best fit with an intercept passing through the origin is 2.58 ($R^2 = 0.9464$) and 6.0422 ($R^2 = 0.9824$) for $d_p = 2.6$ and 10.6, respectively.

In the same way that the estimated SSC for the base scenario was scaled by the slope of the line of best fit through the SSC estimates, the SSC estimates produced with the changed d_p were scaled by the slope of the line of best fit through the SSC estimates. The percent difference between the corrected SSC and the known SSC is presented in table 2.4 along with the base scenario with a d_p of 6.6 μm. Reducing the primary particle size by 61% from 6.6 μm to 2.6 μm causes an average percent difference in corrected SSC of 11.4%. The largest observed percent difference is 28.4%, which occurred for a d_p of 2.6 μm for the 100 mg/L test at a mixing rate of 90 Hz. Increasing d_p by 61% to 10.6 μm results in an average

percent difference in uncorrected SSC of 7.8%. The average percent difference for the base case where $d_p = 6.6$ μm is 7.2%.

Table 2.4: Percent difference of linearly scaled corrected SSC estimates from the actual SSC for different values of d_p

Actual SSC [mg/L]	Mixing rate [Hz]	% difference d_p [μm] 2.6	6.6	10.6
20	50	5.0	7.4	13.2
20	90	17.4	1.7	5.7
100	50	13.9	0.2	7.0
100	90	28.4	17.6	12.4
200	50	0.4	7.8	11.7
200	90	17.4	9.6	5.7
300	50	1.2	2.9	4.0
300	90	22.8	15.6	12.0
400	50	3.9	1.0	0.2
400	90	0.9	3.2	5.2
500	50	17.7	10.9	7.4
500	90	7.4	8.0	8.5

The model presented here for estimating SSC from particle data collected with the FlocARAZI camera system was developed by taking the characteristic primary particle diameter as the median particle size of the test sediment and assuming a density of 2500 kg/m^3. Since the proposed model includes linearly scaling the uncorrected SSC by a known SSC measurement, the input parameter ρ_0 has no consequence on the final corrected SSC output from the routine. Specifying ρ_0 simply provides a starting point for estimated SSC that will be corrected by a physical measurement, or to provide relative concentration estimates between a series of deployments with the FlocARAZI. The choice of d_p, however, influences both the magnitude and, to a lesser extent, the shape of estimated SSC as shown in figure 2.6. The difference in magnitude will be accounted for when linearly scaling the uncorrected SSC. Though, the difference in shape is not accounted for with the linear scaling. Therefore, the

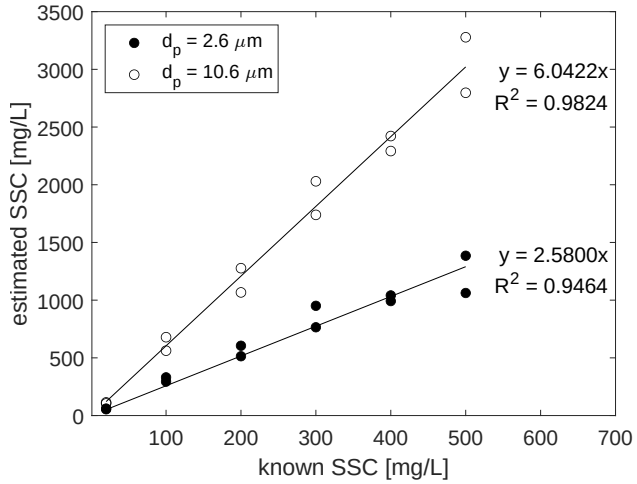

Figure 2.6: Estimated SSC and line of best fit for two different values of d_p while maintaining $\rho_0 = 2500$ kg/m^3.

importance of the specified value for d_p should be considered when a wide range of SSC and floc sizes are observed. The tests presented here show that within a range of d_p values that could be reasonably observed in nature, the response of the model to changes in d_p is close to linear.

2.7 Identifying sand within particle data

When deploying the FlocARAZI in a high energy sand-bed river such as the Mississippi River, sand grains are likely to be in suspension and imaged as part of the suspended load along with flocs. Therefore, a method for identifying sand grains within the image data is desired to allow for analysis of the mud data separated from the complete data set.

To achieve the separation of sand particles from mud aggregates of similar size, we used an optimizable support vector machine (SVM) binary classifier within the MATLAB Classification Learner Toolbox. SVM is a supervised machine learning algorithm that attempts to classify data by finding the hyperplane that best separates the two classes. The hyperplane is a flat (n-1)-dimensional subspace within the n-dimensional space, where n is equal to the

number of characteristics provided to the classifier to describe the data (Noble, 2006). For example, the characteristics from the particle data could include area, perimeter, aspect ratio, etc. In addition, SVM can separate nonlinear data by including a kernel function, where the kernel function allows for transforming the data to a higher-dimension feature space and fitting a hyperplane within the higher-dimensional feature space. The resulting higher-dimensional hyperplane can then be mapped to the original n-dimensional space, resulting in a non-linear curve or non-flat surface separating data classes within the n-dimensional space, for n = 2 and n = 3 and greater, respectively. A trained SVM model can then classify new data based on which side of the curve or surface the new data is located.

2.7.1 Data preparation

Particle data from images collected both in the field and in the lab were used for the training and testing of the SVM. The field data is from images collected on the lower Mississippi River near the Bonnet Carré Spillway (BCS) in December 2019. This area of river is characterized by a subaqueous sand bar that runs adjacent to the BCS, which is positioned immediately downstream on the inside of a bedrock bend (Nittrouer et al., 2012). Images for this analysis were collected both over the thalweg within the bend and over the subaqueous sand bar. Laboratory data was included to train the model with an extended range of floc and sand data past what was observed in the field. The lab floc data came from the tests performed for the concentration estimation experiments. Additional sand particle data was obtained by sieving bed sediment, originating from the New River near Radford, VA, through seven mesh sieves, ranging in size from 63 μm to 500 μm. Sand from each sieve was imaged and the processed data was included with the training data. Each particle from the lab and field data was then identified as being either sand or not sand, represented by a one or zero, respectively. For sand grains, any particle smaller than 63 μm was considered to not be

sand. The resulting combined data set consisted of 852 sand particles and 13,372 non-sand particles. The combined data set was then split with 80% into a training set and 20% into a testing set.

2.7.2 Training and testing SVM classification model

Training the optimizable SVM model consisted of importing the training data set into the MATLAB Classification Learner App, selecting a model validation method, selecting which features to train the model with, and optionally performing a principal component analysis on the selected features to reduce the feature space. In addition, optimizable components of the model include the kernel function, box constraint level, kernel scale, and standardization of the data. For the developed model, an initial Principal Component Analysis (PCA) revealed that the majority of information is provided by the area, perimeter, major and minor axis of an ellipse fit around the particles, and the contrast of the particle. Therefore, these features were selected as the training features, with the remaining features excluded. These five features were then passed through the PCA within the classification learner app, and three of the principal components were retained. The reduced particle data, within the principal component space is then used as the particle characteristic data that defines the location of sand and non-sand particles within the hyperspace. A Gaussian kernel function and the option to standardize the data were selected. The SVM box constraint level and kernel scale were selected as optimized parameters. That is, the Classification Learner App automatically selects and tests different combinations of values for the box constraint and kernel scale, and updates the optimized parameters based on a selected optimizer, in this case Bayesian optimization was selected. Finally, 5-fold cross-validation was implemented to gauge the accuracy of the model.

The resulting classification model had a 99.67% accuracy with the training set. Applying

Table 2.5: Results from testing the trained SVM model on unseen particle data

Particle type	# of particles	# correctly identified	True positive [%]	False discovery [%]
Floc	2692	2689	99.89	0.15
Sand	153	149	97.39	1.97

the model to the reserved test set produced an overall accuracy of 99.75% and a true positive rate of 97.39% and 99.89% for the identification of sand and non-sand, respectively. The hyperplane developed with the SVM model, within the principal component space, is shown in figure 2.7. The separated floc and sand particle size distributions from the test data set are presented in figure 2.8.

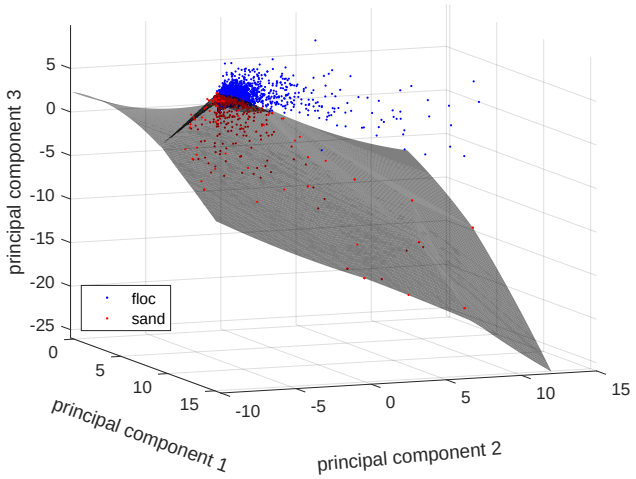

Figure 2.7: SVM developed surface plot separating floc and sand training data within the principal component space for the characteristic data of each particle. This surface will then be used as the boundary to classify unseen data.

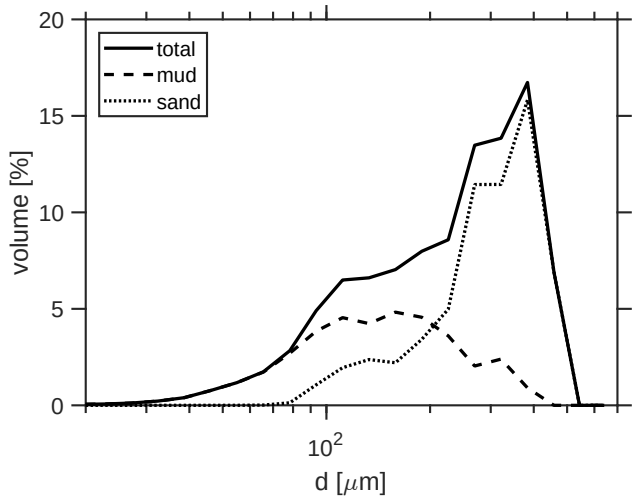

Figure 2.8: Volume-based particle size distributions for the floc and sand fraction and combined distribution. The distributions data is taken from the classification test data set.

2.8 Discussion

2.8.1 Comparison of FlocARAZI with other in-situ cameras

The relatively simple nature of the construction of the FlocARAZI allowed for development of an in-situ particle sizing system that can be constructed with the cost of parts at less than $4000 USD. The direct video stream to the surface provides the user the ability to know the condition of suspended sediment and image quality in real time. If images are out of focus, the stepper motor controlled platform, on which the camera is mounted, can be easily re-positioned while the FlocARAZI is deployed. With improvements in digital camera sensor technology over the past two decades, the FlocARAZI is able to collect high resolution 4000 x 3000 pixel images at a collection rate up to 10 frames per second with a compact and easy to handle form factor. In contrast to other particle sizing devices with a flow-through cell design, the DFC and InSiPID imaging devices have a resolution of 1024 x 1024 pixels and 659 x 494 pixels, respectively. Additionally, compared to the DFC, InSiPID, and PICS, which use a flashed light source that requires syncing with image acquisition, the FlocARAZI

uses a continuously illuminated light source, reducing complexity and potential sources of equipment malfunction. Due to the compact nature of the system, a second camera and lens assembly could be added to the system with a different flow-through cell gap width, similar to the InSiPID camera system, to increase the range of observable particle sizes, depending on the intended application.

An additional benefit of the flow-through cell design utilized by the FlocARAZI is the ability to collect a large number of independent floc observations in a short period of time while profiling, when compared to imaging systems that rely on imaging flocs within a settling tube at discrete locations over the water column. For example, profiles with the PICS system have been reported to collect around 6,000 particle observations for a single profile consisting of seven sampling depths at a station with a total depth of 13.6 meters. This profile took approximately 22 minutes. In comparison, during a profile within the Mississippi River that took 14 minutes at a station with a depth of 16 meters, the FlocARAZI captured 1162 images and 111,902 in focus particles, with 51,672 of those particles being larger than 30 μm. However, while the FlocARAZI is capable of collecting a large number of independent floc observations in a short amount of time, settling tube systems such as the PICS do provide needed floc settling velocity and hence floc density information. Therefore, an ideal system would combine both the FlocARAZI and a system like the PICS to obtaining both a large number of independent floc size observations and floc settling velocity information.

2.8.2 SSC correction factor

A common method for estimating SSC within aquatic environments is to relate SSC from physical samples to turbidity measured by an OBS. Others have estimated SSC with LISST instruments by simply assuming that the measured sediment only consists of dispersed minerals with a particular density. However, Sequoia Scientific warns that this method is not

accurate if flocculation, organic matter, or minerals of variable density are present in the environment where measurements are obtained. Therefore, estimating SSC with an image-based approach provides a unique opportunity to collect both particle size, type (flocculated or unflocculated), and SSC with a single instrument. To the best of our knowledge, only one other researcher has attempted to estimate SSC from a microscope-lens, image-based method (Antonenkov, 2016). Antonenkov (2016) developed an algorithm for identifying sand grains within images and related the pixel area of the sand grains to an equivalent circular diameter. The volume of the sand was then assumed to be equal to the volume of a sphere of the equivalent circular diameter and the mass was estimated by assuming a constant density for all sand grains. The SSC was then estimated as the sum of the mass of observed sand divided by the volume of the observable field field of view for the collected images. This method corresponds exactly to the approach we take for estimating the contribution of sand to the total SSC estimate. Though, the work presented here expands upon the work of Antonenkov (2016) to include a method for estimating SSC when flocs are present in suspension and for improving the accuracy of SSC estimates for particles in the smaller size ranges through the use of a variable sample width that is dependent on particle size.

The utilization of a correction factor for estimating SSC accounts for a number of model parameters that have inherent variability. Such parameters include the empirically derived relation used to obtain N_{f3} from N_{f2}, the use of a single characteristic d_p, estimating floc volume as the equivalent spherical volume, and variability in primary particle density. Consequently, SSC estimates from images collected with the FlocARAZI in the field will need to be calibrated against a measured SSC by use of a linearly scaled correction factor. An additional result of using a correction factor is a reduction in the influence of the specified values for d_p and ρ_0 on the final corrected SSC values.

The method we introduced for estimating SSC with the FLocARAZI has been used to estimate SSC from images collected in the Mississippi River. The method has produced

reasonable estimates without the use of the correction factor for calibration, producing a similar SSC profile to physical water samples collected with an isokinetic sampler. Using the physical water samples as a calibration provided the means for estimating SSC for profiles collected with the FlocARAZI at other locations during the survey where time constraints or flow conditions prohibited collection of physical water samples.

2.8.3 Sand identification dependence on image exposure

Observing suspended sediment characteristics with an image-based device provides the unique opportunity to visualize and characterize the particles that make up the calculated particle population statistics. Compared to non-optical particle sizing instruments, particle sizing with an image-based device such as the FlocARAZI provides the information necessary for training a machine learning algorithm for identify sand within the population of observed particles. The ability to identify sand within the observed particle population is a significant advancement for floc research in fluvial environments where both flocs and sand are present in suspension. As a result, floc population characteristics can be calculated directly without making additional measurements and assumptions that would be necessary in the case of laser diffraction based particle sizing instruments or physical water samples where flocs are not observed directly.

Since the identification of sand with the SVM model relies on the contrast of the identified particles and their geometric properties, accurately distinguishing sand from other particles depends on the exposure conditions under which the images were taken. As a result, when deploying the FlocARAZI, a standard operating procedure for setting the LED intensity needs to be implemented to match the image exposure conditions under which the SVM model was trained. If exposure conditions are not similar, a new SVM could be trained or the data used to train the existing SVM could be combined with the new data to train a

new model that is, ideally, more robust to variations in exposure conditions.

2.9 Conclusions

This paper presents the system components, packaging, and validation of an inexpensive and compact field-deployable camera system designed to image flocs in-situ. The use of an automated image processing routine and a method to obtain 3D fractal dimensions from 2D images were combined to estimate SSC of flocculated sediment from image data collected with the FlocARAZI. Additionally, a SVM machine learning model was introduced to identify sand grains within particle data collected with the FlocARAZI, providing the means to calculate floc size characteristics independent of suspended sand.

The FlocARAZI system and image processing code was designed to be a cost effective and easily reproducible solution for imaging flocs in-situ within the fluvial and marine environment. In accordance with the hope that developing a lower cost alternative to particle sizing instruments currently on the market will allow for an ever-increasing number of field observations of flocs; As part of this effort, the parts list for the FlocARAZI, build instructions, and image processing code are publicly available here:(a GitHub address will be added if the paper is accepted for publication).

Chapter 3

Vertical profiles of floc size and mud concentration in the lowermost reaches of the Mississippi River

Ryan Osborn[1], Kieran B.J. Dunne[2], Ehsan Abolfazli[1], Jeffrey A. Nittrouer[2], and Kyle Strom[1]

[1]Civil and Environmental Engineering, Virginia Tech, Blacksburg VA USA

[2]Rice University, Department of Earth, Environmental, and Planetary Sciences, Houston, TX, USA

Manuscript in preparation for submission to *Journal of Geophysical Research: Earth Surface*.

3.1 Abstract

This study focuses on presenting field observations of flocculated suspended sediment size and concentration over the water column within the lowermost Mississippi River. The research questions that are explored include: is mud flocculated within the freshwater reaches of the lowermost Mississippi River, how is floc size and mud concentration distributed over the water column within freshwater and stratified sections of the river, and does the presence of flocs lead to vertical stratification of the mud concentration? Floc size data from the freshwater main channel and the vertically stratified salt wedge distributary, Southwest Pass (SWP) are presented and analyzed. A Rouse profile was fit to the mud fraction of suspended sediment concentration to investigate influence of flocculation on vertical gradients in mud concentration over the water column. Field surveys in summer 2020 and winter 2021 were conducted at three distinct zones along the lowermost Mississippi River. Namely, the Mississippi River station locations included: the high energy channel near the Bonnet Carré spillway (BCS); Venice, Louisiana, (VMC) immediately upriver from the first of seven major distributaries within the delta; and Southwest Pass (SWP), the major distributary and shipping passage. Floc size and concentration information over the water column was collected with the FlocARAZI, a new, in-situ microscope imaging device. At the BCS and VMC, average floc sizes were observed to range from approximately 75 to 200 μm during the summer and 45 to 125 μm during the winter. In addition, at the BCS and VMC, flocs size distributions tended to show fining of flocs near the bed compared further up in the water column, indicating that floc size could be reduced due to higher turbulence levels near the bed. Floc sizes within SWP were observed to be relatively uniform, between 60 to 100 μm, within the upper freshwater and lower marine layer of the salt wedge. However, the largest average floc sizes, just under 600 μm, were observed within the mixing layer between the freshwater and marine layers. Estimated bulk settling velocities from the Rouse profile

analysis range from around 0.08 mm/s at the BCS during the winter to 2.86 at SWP1 during the winter. Bulk settling velocities for flocs at the BCS and VMC during the summer survey range from around 0.42 mm/s to 0.52 mm/s. Overall, average floc sizes are observed to vary seasonally and by longitudinal location within the Mississippi River.

3.2 Introduction

Many populated coastal areas are currently experiencing an ever increasing amount of land loss as a result of relative sea level rise, a reduction in sediment supplied to coastal floodplains, and an increase in frequency and intensity of coastal storm events (Morton, 2003; Kulp and Strauss, 2019; Bird, 1996). In addition, sediment loads supplied by rivers to coastal zones is changing as a result of land use changes within drainage basins, river alteration, and other anthropogenic forcing resulting in changes in sediment inputs (Walling and Fang, 2003). As a result, in many coastal areas, the supply of sediment is not in balance with erosion causing a retreat of coasts, which has lead to a loss of habitat for coastal species as well as reducing the buffer zone for inland storm surge during extreme storm events (Kennish, 2002; Sheng et al., 2012; Möller et al., 2014). Recently, studies have investigated potential solutions for enhancing coastal resiliency to prepare for a future that would otherwise consist of persistent land loss if no action is taken (Nordenson et al., 2018). One potential solution that has been proposed is the construction of sediment diversions (Nittrouer et al., 2012; Esposito et al., 2017; Xu et al., 2019). Though, the planning of such projects will require extensive modeling of suspended sediment dynamics to predict the potential for land building from diverted water and sediment. A major component of suspended sediment in large rivers is the mud fraction consisting of clay and fine silts that have the potential for aggregating into larger units know as flocs. Flocculation of mud in estuarine and marine environments has been extensively explored relative to the fluvial environment. However, little is known

about the extent of controls on flocculation in the fluvial environment, such as turbulent shear rate, freshwater ion content, biological activity, and sediment composition. Though, a better understanding of these controls will be necessary for accurate modeling of mud transport and sedimentation both within the freshwater environment and as an upstream boundary condition for mud entering the estuarine environment.

Understanding mud transport and deposition processes has been widely recognised as important for maintaining navigable waterways, understanding delta formation, and reconstructing marine geological records (Einstein and Krone, 1962; Krone, 1962; Potter et al., 2005; Schieber et al., 2013). Though, the complicating factor in modeling mud transport is the ability of silts and clays to aggregate into flocs with densities less than that of their constituent particles. In particular, the dependence of floc density on environmental factors that vary by location and in time such as turbulence levels, salinity, organic content, and sediment properties poses a problem in accurate modeling of mud transport, and consequently requires in-situ observations to inform modeling efforts. Many field studies have been conducted to characterize floc size and settling velocity in the estuarine and marine environments. Within the estuarine and marine environment, flocs have been observed to range in sizes from tens of microns up to five to eight millimeters, with settling velocities from 0.01 to 22 mm/s (Fennessy et al., 1994; Dyer et al., 1996; Hill et al., 1998; Fox et al., 2004; Manning et al., 2006; Winterwerp et al., 2006; Mikkelsen et al., 2007; Guo et al., 2017). However, little focus has been placed on characterizing floc size in the freshwater fluvial environment.

The research questions that motivated this work include: (1) Is mud flocculated within the high energy environment of the laterally confined freshwater section of the lower Mississippi River? (2) If flocs are present within the laterally confined freshwater zone, how does floc size vary over the water column and can this variation in floc size explain observations of concentration gradients in the mud fraction of suspended sediment in water samples col-

lected in past studies? and (3) How does floc size vary over the water column in the presence of a salt wedge? To explore these questions, the FlocARAZI, a camera-based in-situ imaging device was used to obtain direct observations of suspended sediment characteristics over the water column in these key zones of the Mississippi River (Osborn et al., 2021).

3.3 Survey location and background

Surveying trips were conducted during summer (June 24 through July 2 of 2020) and winter (January 9-14, 2021). Both trips consisted of data collection at three key locations along the lower Mississippi River Delta, namely the Bonnet Carré Spillway (BCS) (Fig. 3.1a), the main channel 2 km upriver from the Baptiste Collette distributary, herinafter referred to as Venice Main Channel (VMC), and at select locations along Southwest Pass (SWP) (Fig. 3.1b). During the summer survey, data were collected at two locations along a lateral transect at the BCS and three locations at VMC. The winter survey consisted of data collection at one location within the thalweg at both the BCS and VMC, and 6 stations along SWP starting approximately 3 km downriver from Head of Passes, and ending approximately 27.5 river kilometers downriver from Head of Passes. Discharge data was acquired from USGS station 07374000 at Baton Rouge, LA. During the summer survey, the river discharge was on the receding limb from a peak of just over 28,300 cms. Over the duration of the survey, the discharge dropped from 22,600 cms on June 24 to 16,500 cms on July 2. The average daily water temperature during the summer survey was 27.4 degrees Celsius. In the five months prior to the winter survey discharge did not exceed 13,500 cms. Discharge then started to increase from 12,000 cms on January 2, surpassing 13,500 on January 4. During the period of data collection discharge rose from 17,000 cms on January 9 to 19,800 cms on January 14. The daily average water temperature during the winter survey was 6.3 degrees Celsius.

During periods of low discharge, around 8,500 cms and lower, a salt wedge consisting

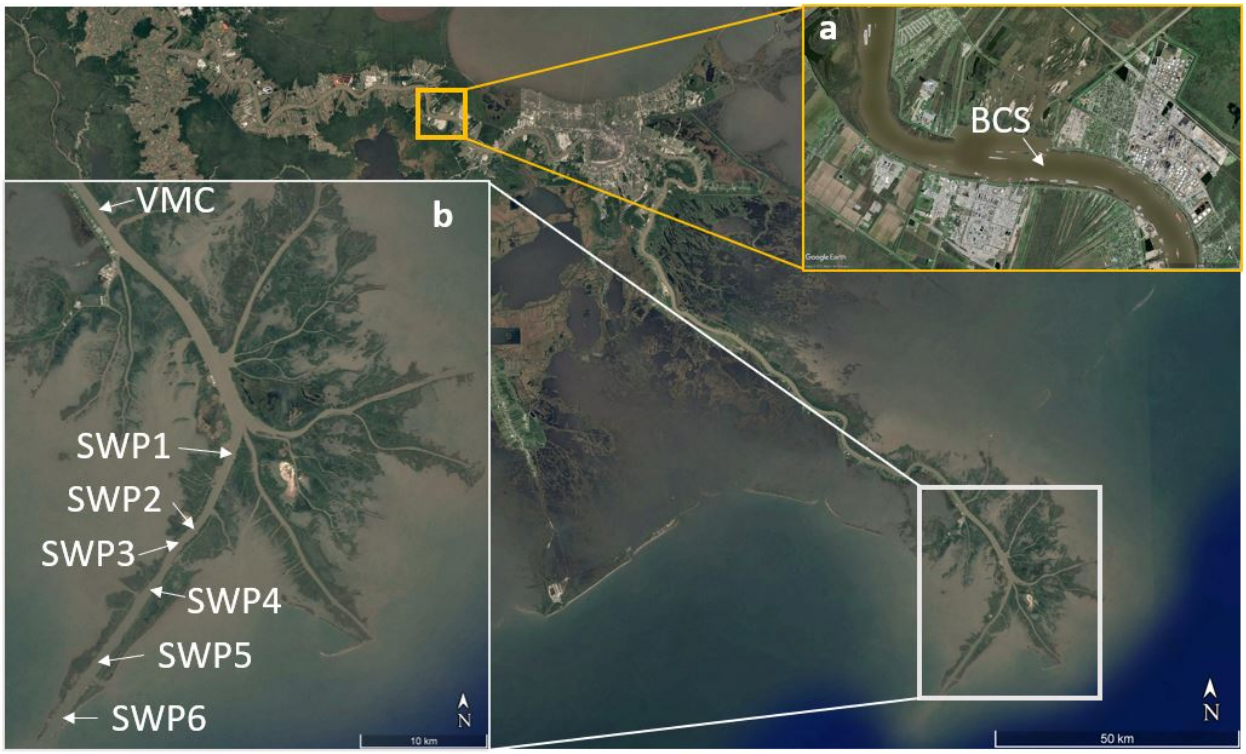

Figure 3.1: Survey locations. (a) Bonnet Carré Spillway (BCS). (b) Mississippi River Delta, including stations VMC and SWP 1-6.

of Gulf of Mexico water has been observed to migrate upriver of Head of Passes (Galler and Allison, 2008). Galler and Allison (2008) found that while the salt wedge is in place, accretion rates, consisting mainly of mud, have been observed to range from 1.7 mm/day to 8.9 mm/day, with the thickest mud deposits being up to 3 m deep within the thalweg. With the high discharge during the summer survey, the salt wedge was observed to be confined to SWP. During the summer survey, the bed material consisted mainly of sand at all three locations, including within the salt wedge within SWP. In contrast, except for the BCS bed sample, bed material for the VMC and SWP locations consisted mainly of mud during the winter survey. However, the salt wedge was also observed to be confined within SWP during the winter survey. From November 20 to January 1, the average discharge at the Baton Rouge USGS station was 12,000 cms, with a peak of 12,650 cms and a low of 11,000 cms.

This period of low discharge could have potentially allowed for upriver migration of the salt wedge past the VMC station, with retreat of the salt wedge as discharge increased leading up to and during the survey period.

3.4 Methods

3.4.1 Field measurements

Collected data at all stations includes: particle size and concentration information from the Floc AReA and siZing Instrument (FlocARAZI) imaging system (Osborn et al., 2021); conductivity, temperature, and depth with a Sontek CastAway CTD deployed with the FlocARAZI; and water velocity data with a Teledyne RiverPro acoustic Doppler current profiler (ADCP). At each longitudinal location within the thalweg, isokinetic water and sediment samples were collected with a USGS P-63 and bed material samples were collected with a Shipek grab sampler.

The FlocARAZI imaging system was designed to image flocculated suspended sediment in-situ over the water column at depths up to 60 meters, identify sand within particle data, and estimate mass suspended sediment concentration (SSC) from image data. During deployment, a live video feed from the camera is transmitted via a Cat6 ethernet cable to a laptop at the surface where images are saved to the hard drive. A Sontek CastAway CTD is attached to the frame of the FlocARAZI, providing conductivity, temperature, and depth information by matching image timestamps with CTD data timestamps. The FlocARAZI systems consists of a camera, microscope lens, and LED light source situated within a waterproof housing. The camera system has a field of view of 3.7 x 2.8 mm and can resolve particles down to 6 microns. Suspended sediment is allowed to pass freely through a flow-through cell with a gap width of 1.17 mm. Images collected with the system are processed

following the image processing routine developed by Keyvani and Strom (2013), with slight modifications outlined in Osborn et al. (2021). The relevant output from the image processing routine is the particle area in pixels^2, which is converted to an equivalent circular diameter.

The particle diameter is converted from pixels to microns with 0.925 microns/pixel conversion factor. A processing routine utilizing a trained Support Vector Machine (SVM) classifier allows for identifying sand particles within the full particle data set, providing the means to isolate and analyze the flocculated and silt fraction of suspended sediment separate from the full imaged particle data set. Estimating mass SSC with the FlocARAZI data was performed following the methods developed in Osborn et al. (2021), where calibration of the estimated SSC was achieved by scaling SSC estimates from the FlocARAZI with SSC measurements obtained from P-63 water samples.

During deployment of the FlocARAZI, images are collected at a frequency of 2 Hz. With the CTD sampling initiated, the camera system is lowered in 3 meter increments starting at the surface and lowered to within 1-3 meters of the bed depending on variability of the bed elevation. At each increment over the water column, the FlocARAZI position is held steady for 1-2 minute to collect approximately 90 images suitable for processing. In areas of interest such as the mixing zone between the freshwater and saltwater interface of the salt wedge in SWP, the FlocARAZI is lowered in 1 meter increments. While the FLocARAZI is deployed, the boat is throttled to minimize the velocity difference between the boat and the fluid at the location of the camera.

Isokinetic water samples were collected with a USGS P-63 to measure SSC. Collecting water samples consisted of holding the boat position steady, lowering the P-63 to a predetermined depth, and opening the solenoid valve to fill a 1-L sample bottle. The solenoid is opened for a period of time ranging from 10 - 60 seconds depending on current speeds, allowing for the sample bottle to fill to approximately 75% capacity, ensuring the sample

bottle is not overfilled during sampling. Samples were collected at 5%, 25%, 50%, 75%, and 95% of the station flow depth from the bed. Water samples were filtered on site with 1 μm glass fiber filters and the liquid volume of the sample recorded. Once back to the lab, filtered water samples were allowed to dry in an oven at 80 degrees Celsius for 24 hours. The sample and filter were then weighed and the mass of the filter subtracted to obtain the mass of the sample.

Bed material samples were collected at each station with a Shipek grab sampler. Samples were processed by first mixing the sediment until homogeneous. A subsample of the homogenized sample was then wet sieved with a No.230 (63 μm) mesh sieve to separate the fine and coarse sediment. The grain size distribution of the coarse fraction was obtained by sizing with a Retsch Technolog CAMSIZER.

While the FlocARAZI was deployed, velocity profiles were collected continuously with a Teledyne RiverPro Acoustic Doppler current profiler (ADCP). Velocity profiles were collected at an average sampling rate of 0.47 Hz. The method for calculating shear velocity, u_*, included taking the average flow velocity, U, at each depth interval against the natural log of the distance from the channel bed, z. A linear regression was then fit, and the slope of the resulting line was multiplied by the von Karman constant, $\kappa = 0.41$, to obtain the shear velocity associated with each sampling location.

3.4.2 Rouse profile analysis

Within the context of suspended load transport within rivers, the Rouse profile analysis is a simple method for estimating sand concentration profiles given channel geometry and a reference concentration near the bed. In this traditional analysis, the mud fraction (particles smaller than approximately 63 μm) is assumed to be disaggregated and distributed uniformly over the water column as a result of the small fall velocity, and consequently, little to no

net downward flux of sediment, sustained by vertical turbulent fluctuations. As a result, the mud fraction is ignored and the analysis is only applied to the sand fraction of suspended sediment. However, flocculation of mud can increase the settling velocity of the aggregate relative to the individual primary particles. This increase in settling velocity could impact the mud concentration profile over the water column within a river. To investigate the research question of how flocculation impacts the mud concentration profile within the Mississippi River, a Rouse profile was fit to the mud fraction of suspended sediment.

Under steady and uniform flow conditions, equilibrium transport conditions, and by assuming that the net downward flux of suspended sediment is in balance with the upward flux of sediment driven by turbulent motion in the vertical direction, Rouse (1939) developed the well known model for the distribution of suspended sediment. The Rouse distribution for suspended sediment concentration, C, is given as:

$$\frac{C}{C_b} = \left[\frac{(z-H)\,b}{(b-H)\,z}\right]^{Z_R} \tag{3.1}$$

where H is the depth of the water column, C_b is the suspended sediment concentration at the reference height b above the bed, and C is the suspended sediment concentration at the elevation z above the bed. The exponent Z_R is the Rouse number:

$$Z_R = \frac{w_s}{\alpha\kappa u_{*s}} \tag{3.2}$$

In equation 3.2, w_s is the settling velocity of particles in suspension, κ denotes the von Karman constant, taken as 0.41, u_{*s} is the portion of shear velocity that results from skin friction drag, and α is a coefficient that accounts for reduced mixing of momentum and sediment in the vertical as a result of turbulence damping produced by sediment stratification. It was found by Wright and Parker (2004a) that stratification effects are most significant for

large, low-slope rivers. Here stratification effects were accounted for through the relation developed by Wright and Parker (2004b):

$$\alpha = \begin{cases} 1 - 0.06\left(\frac{C_{5t}}{S_0}\right)^{0.77} & \text{for } \frac{C_{5t}}{S_0} \leq 10 \\ 0.67 - 0.0025\left(\frac{C_{5t}}{S_0}\right) & \text{for } \frac{C_{5t}}{S_0} > 10 \end{cases} \tag{3.3}$$

where C_{5t} is the is the volume concentration of suspended sediment at 5% of the flow depth from the bed, and S_0 is the water surface slope.

When bedforms are present in the channel, the total shear stress, and hence the shear velocity includes both the effect of skin friction and form drag. However, only the skin friction portion of shear stress is responsible for transporting sediment. Since bedforms were present at the BCS and VMC locations during the summer and at the BCS location during the winter, the shear velocity associated with skin friction will need to be calculated for these locations. Again, a relation developed by Wright and Parker (2004b) for estimating skin friction shear stress, τ_{*s}, in large, low-slope rivers is used, where:

$$\tau_{*s} = 0.05 + 0.7(\tau_* Fr^{0.7})^{0.8} \tag{3.4}$$

In equation 3.4, τ_* is the total dimensionless bed shear stress, and Fr is the Froude number where $Fr = U/\sqrt{gH}$. Witin the Froude number, U is the depth averaged velocity obtained from ADCP measurements, and H is the total depth at a particular station. By definition, the total dimensionless bed shear stress is obtained from:

$$\tau_* = \frac{u_*^2}{gR_s d} \tag{3.5}$$

where g is the acceleration due to gravity, d is the characteristic grain size, taken here as d_{50}, and R_s is the submerged specific gravity, given by $R_s = (\rho_s - \rho)/\rho$ where ρ_s is the density

of the sediment, and ρ is the fluid density.

3.4.3 Theory - Settling velocity from flocculation model

Modeling the settling velocity of suspended sediment necessitates the need for settling velocity relationships that can describe the settling behavior of suspended particles. Flocs are particularly difficult to model due to their irregular shape, porous nature, and variable density. As such, settling velocity relationships, separate from those used for coarse silts and sands, are required for estimating floc settling velocity.

The settling velocity model developed by Strom and Keyvani (2011) was used to investigate expected settling velocities from floc data obtained from the surveys. The model is a modification of the settling velocity equation proposed by Ferguson and Church (2004) and is designed to work under both inertial and viscous settling conditions using the assumption that a floc of size d_f is a 3D fractal aggregate composed of primary particles of size d_p,

$$w_s = \frac{gR_s d_f^{N_{f3}-1}}{b_1 \nu d_p^{N_{f3}-3} + b_2 \sqrt{gR_s d_f^{N_{f3}} d_p^{N_{f3}-3}}} \tag{3.6}$$

In equation 3.6, ν is the kinematic viscosity of the fluid. The coefficients b_1 and b_2 act as calibration coefficients that account for floc shape, permeability, and impacts from drag within the inertial range (Strom and Keyvani, 2011). Strom and Keyvani (2011) fit the model to a wide range of experimental and field floc data to obtain best fit values for b_1 and b_2. Strom and Keyvani (2011) observed the best correlation between the settling velocity curve and data when $N_{f3} = 2.5$, $b_1 = 100$, and $b_2 = 0$.

3.4.4 Data used in the analysis

Parameters needed for the Rouse profile analysis includes water column SSC measurements over the vertical, including a SSC measurement at a reference height, a measure of shear velocity for the station, and a measure of sediment stratification to account for the effects of turbulence damping.

For the analysis here, SSC measurements were made with the FlocARAZI following the methods presented in Osborn et al. (2021). For the summer survey, only SSC measurements made with the FlocARAZI are used in the analysis, as no water samples collected with the P-63 are available to be included in the analysis. The correction factor used for the SSC estimates from the summer survey were derived from an average of the correction factors used for the winter survey stations. For the winter surveys, SSC measurements were collected at all three stations included in the analysis (BCS, VMC, SWP1). For all three stations, the SSC measurements made with the P-63 were used to inform the correction factor needed for FlocARAZI SSC measurements. The correction factor for each station was obtained by visually observing the best fit, by trail and error, between the SSC measured with the P-63 and those estimated by the FlocARAZI. During the winter survey, a large amount of sand was present in suspension at the BCS. Therefore, the correction factor for the FlocARAZI SSC measurements was obtained by fitting the P-63 SSC measurements to the total SSC estimated, including both mud and sand, with the FlocARAZI. Little sand was observed in suspension at the VMC or SWP1 stations during the winter survey, as such, both the SSC measured with the FlocARAZI and P-63 water samples are assumed to contain little to no sand. For the summer survey, the reference depth and SSC were taken as the lowest depth where a SSC measurement was collected. For the winter survey, the same method used for the summer survey was employed for the BCS station, however, SSC measurements made with the P-63 sampler were used as the 5% reference SSC at the VMC and SWP1 stations.

ADCP velocity data collected at all stations was used to obtain shear velocity estimates. When no bedforms are present the shear velocity can be taken as the shear velocity estimated from a log-law profile fit to the ADCP velocity data. Since no bedforms were present during the winter survey at VMC and SWP1, influences of form drag on shear velocity is assumed to be minimal. To account for the impact of bedforms at both BCS and VMC during the summer survey and BCS during the winter survey, the empirical relation (Eq. (3.4)) developed by Wright and Parker (2004b) was employed to estimate the skin friction component of shear velocity. When using equation 3.4; the velocity input needed for the Froude number was obtained by depth averaging velocity data from ADCP measurements. The dimensionless bed shear stress was calculated by taking $R_s = 1.65$ and using the d_{50} from the bed material samples.

The effect of turbulence damping due to sediment stratification was accounted for by equation 3.3. To use equation 3.3, the volume concentration of sediment at 5% of the flow depth and the water surface slope is needed. The volume concentration of suspended sediment was calculated assuming a sediment density of 2650 kg/m^3 and a water density of 1000 kg/m^3. Estimates of the water surface slope were obtained from Nittrouer et al. (2011), where the authors present water surface slope measurements obtained up river from Head of Passes under varying discharge ranges.

With the shear velocity and stratification parameter constrained, the only remaining variable within the Rouse number (Eq. 3.2) is the settling velocity, w_s. The settling velocity was obtained by performing a least squares regression analysis by fitting a Rouse profile to concentration data obtained from the FlocARAZI and physical water samples (Fig. 3.8), allowing the settling velocity to vary.

3.5 Results

3.5.1 Vertical profiles of floc size

Floc size data was collected with the FlocARAZI at the BCS and VMC locations during both the winter and summer (Fig. 3.2). In addition, during the winter survey, floc size data was collected at 6 stations within Southwest Pass while a salt wedge was in place (Fig. 3.6).

Main channel (BCS and VMC)

During the summer survey, floc size data was collected at two lateral locations at the BCS station, and three lateral locations at the VMC station; indicated in Figure 3.2 a and b as being either the left bank, thalweg, or right bank. Floc size data was collected only at the thalweg location during the winter survey after observing little variation in floc size at lateral locations from summer floc size data.

The d_{50} floc sizes observed at the BCS during the summer range from around 75 to 100 μm near the bed, and 75 to 175 μm further up in the water column (Fig. 3.2a). A slight increase in floc size from the bed to around 75% of the flow depth is present, with a slight decrease in floc size near the water surface for the right bank station. Average floc d_{50} at the VMC location during the summer survey range from around 75 μm to around 135 μm near the bed (Fig.3.2b). Floc sizes from the surface to around 25% of the flow depth are relatively uniform, ranging from around 100 to 150 μm. The largest flocs were observed at the left bank and right bank stations, where the largest d_{50} values were between 175 and 200 μm. d_{50} values at the VMC station during the winter ranged from around 60 μm near the bed to between 50 to 125 μm near the surface (Fig. 3.2d). Floc sizes near the bed vary only slightly, between 55 to 75 μm, compared to further up in the water column where both average d_{50} floc sizes increase and the range of sizes increase.

Though flocs were observed in suspension at the BCS during the winter survey, the

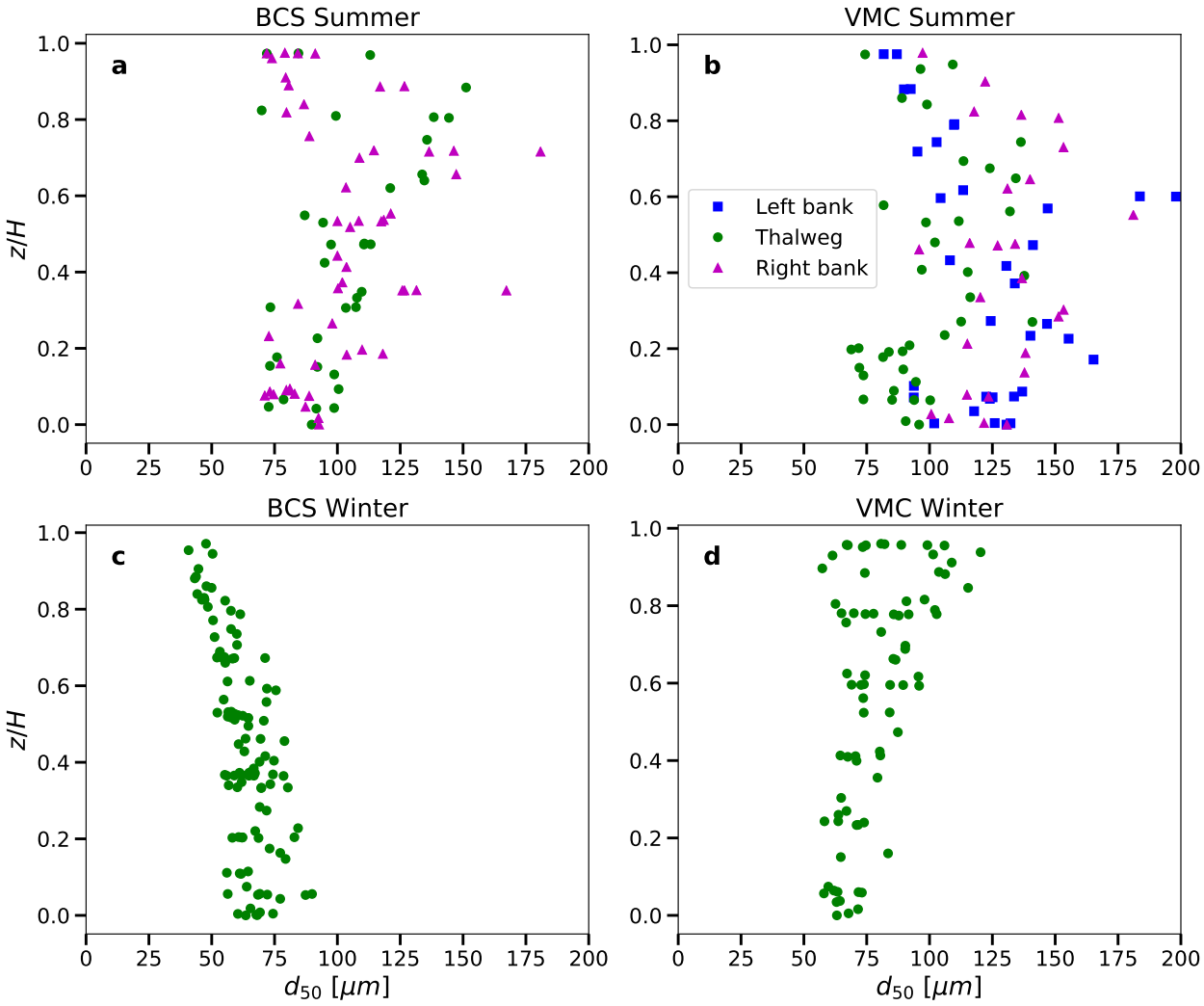

Figure 3.2: d_{50} floc size information collected at the BCS and VMC locations during the summer and winter surveys. Floc size data was collected at multiple lateral locations during the summer survey, as indicated in (a) and (b). Floc size data was collected only in the thalweg during the winter survey(c and d). Though it appears that floc size increases with depth at the winter BCS station (c), this is a result of a large fraction of the observed particles consisting of silt and fine sand. As such, the side information presented in (c) represents the d_{50} of flocs, coarse silts, and fine sands.

Table 3.1: Average floc sizes for main channel stations. *The BCS winter station includes both flocs and fine sand.

Station	d_{16} [μm]	d_{50} [μm]	d_{84} [μm]
BCS Summer	57	102	185
VMC Summer	66	116	213
BCS Winter*	35	63	119
VMC Winter	44	79	160

data presented in Figure 3.2c represents the d_{50} sizes of flocs, silts, and fine sands. This is a result of the turbid conditions and images collected with the FlocARAZI containing a large amount of silt and sand. The algorithm used for identifying sand from image data was unable to correctly identify sand when flocs or silts overlapped with sand within the images. Medium to large sand was manually removed from the data, but the large number of fine sand grains within the data made it unfeasible to manually remove them from the data set. Therefore, the data presented in Figure 3.2c should not be taken to represent only floc sizes at the winter BCS location.

Variation by season: At both stations, floc sizes were larger, on average, during the summer than they were in winter. For example, the average floc d_{50} at the BCS during the summer was 102 μm. In contrast, the average d_{50} of the particles in suspension, which included solid fine sand and smaller, during the winter was 63 μm (Table 3.1). Though, as previously mentioned, the actual d_{50} of the floc sizes at the BCS during the winter are likely smaller than the values presented in Table 3.1 due to the presence of both fine sand and flocs being included in the data presented for this location and time. At the VMC station, the depth averaged d_{50} was 116 μm in the summer compared to 79 μm in the winter. Sample images collected during the summer and winter at the BCS and VMC are presented in Figure 3.3.

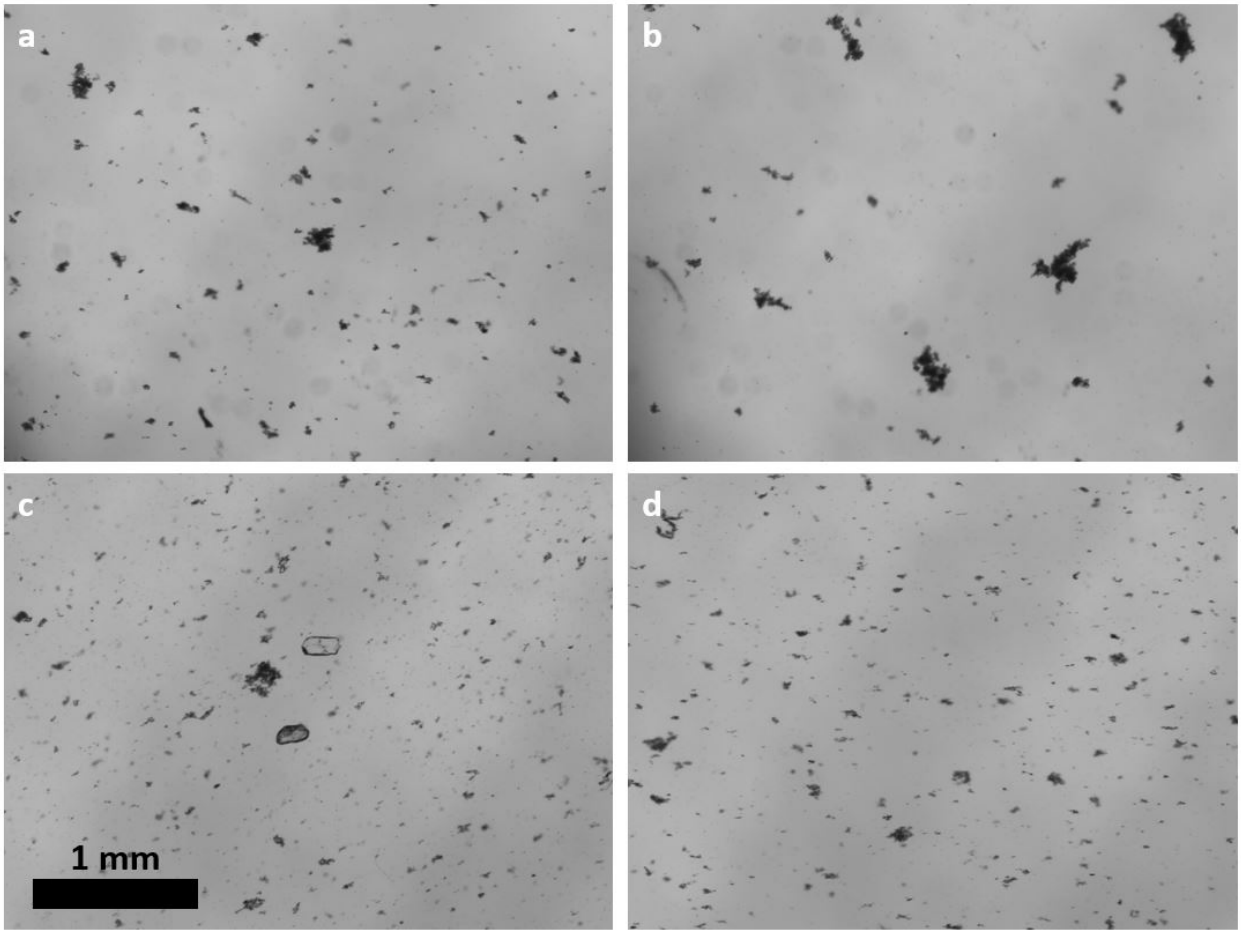

Figure 3.3: Example images collected during the summer at the (a) BCS and (b) VMC, and during the winter at the (c) BCS and (d) VMC.

Population variation over the water column: Floc size, at any given location and time is controlled by turbulence levels and the type and amount of sediment, ions, and organic material present in the water column. While bulk sediment, ion, and organic conditions are not expected to vary significantly over the time period required to collect images with the FlocARAZI within the freshwater reaches of the Mississippi, it is possible for turbulence to vary significantly over the water column. Consequently, it could be expected that floc size population statistics will vary over the water column as a result of adjusting to differences in turbulence conditions.

Variation in floc size population at 7.5%, 25%, 50%, 75%, and 92.5% of the flow depth were investigated by calculating the kernel density estimate (KDE) and the volume percent of flocs in a specified size range for each depth range (Figs. 3.4 and 3.5).

In general, the KDE for all four stations, except for the BCS winter station show an overall fining of floc sizes closest to the bed. This is most clearly depicted by the BCS summer and VMC winter KDE plots (Figs. 3.4 a and d). The VMC summer KDE plots show only slight fining near the bed relative to further up in the water column (Fig. 3.4b). The BCS winter KDE and volume percent of binned particles plots show a coarsening of suspended sediment from the surface to the bed (Figs. 3.4c and 3.5c). Again, this is a result of the data for this particular station representing flocs, silts, and fine sands as previously noted.

The same general trend observed in the KDE plots of the fining of flocs near the bed is also present in the plots presenting the volume percent of binned particles at select locations over the water column (Fig. 3.5). In general, except for the BCS winter station, the volume percent of flocs in the smaller bin size ranges (0 to 100 μm) tend to increase going from the surface to the bed in Figure 3.4. A corresponding decrease in the volume percent of flocs in the larger size ranges (100 to >200 μm) accounts for the increase in the smaller size ranges. Again, the trend of fining of flocs near the bed observed in the KDE plots for the

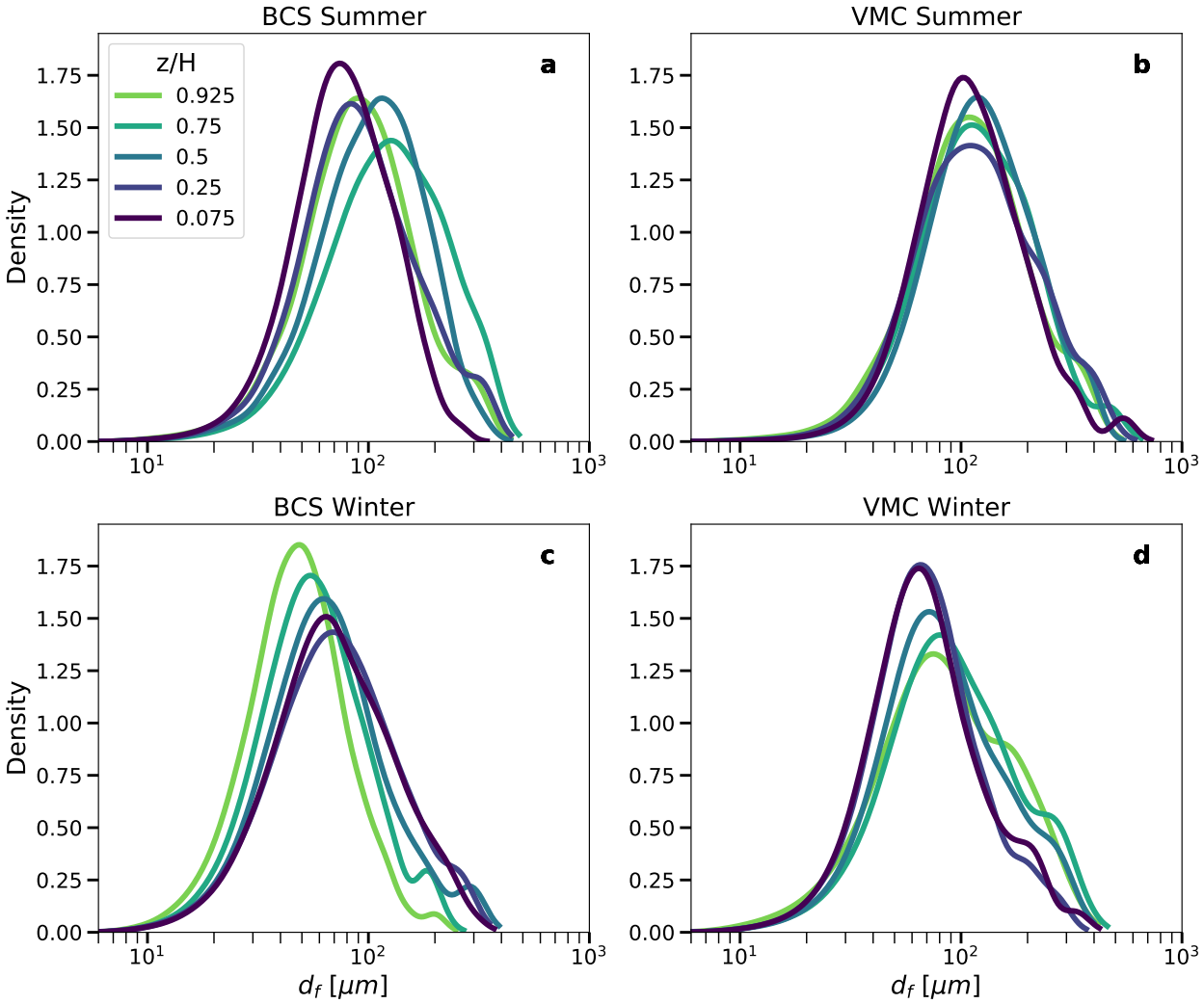

Figure 3.4: Kernel density estimates (KDE) of the probability density function for floc size population data collected over specified ranges within the flow depth. Here z is taken as the vertical distance from the bed and H is the flow depth.

BCS summer and VMC winter stations is observed through an increase in floc volume in the smaller bin ranges (0 to 100 μm) going towards the bed (Fig. 3.5a and d).

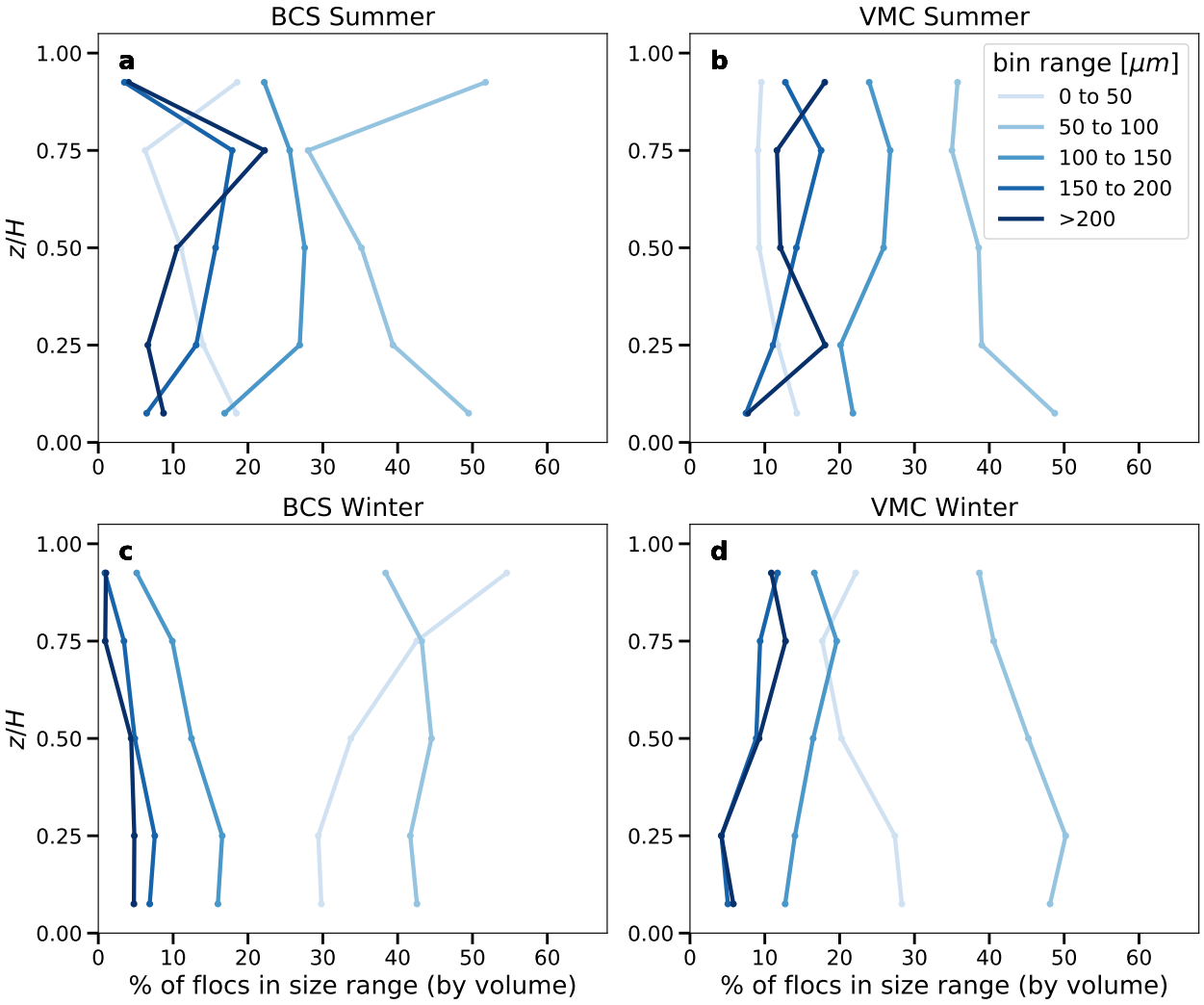

Figure 3.5: Floc size binned by volume into different size ranges at 7.5%, 25%, 50%, 75%, and 92.5% of the flow depth. Here z is taken as the vertical distance from the bed and H is the flow depth.

The volume percent of flocs in the 50 to 100 μm bin range is relatively consistent between the two seasons. The smallest size range (0 to 50 μm) makes up a larger percent of flocs during the winter survey compared to the summer.

Southwest Pass - SWP

Vertical profiles of flocs sizes were also collected within the vertically stratified sections of Southwest Pass during the winter survey (January 9th and 12th, 2021). Overall data collected in this zone spanned from the tip or nose of the salt wedge and progressed through the river mouth. On January 9th the nose of the salt wedge was located approximately 10.5 km down river from Head of Passes (station SWP2). By January 12th the nose had migrated 5 km farther down river (15.5 km from Head of Passes, just down river from SWP4). Vertical profiles of salinity and average floc size just up river of and through the salt wedge in SWP are shown in Figure 3.6. Temperature at each station was observed to follow a similar profile to salinity, where the freshwater temperature was around 7 degrees Celsius and the lower marine layer was around 18 degrees Celsius.

At the most up-river station within Southwest Pass, SWP1, d_{50} floc sizes in the fresh water zone are relatively uniform over the water column and have an average size slightly under 100 μm (Fig. 3.6a). At SWP2, the first observation of the salt wedge is present at slightly less than 20% of the flow depth (Fig. 3.6b). Floc sizes at SWP2 are also relatively uniform both within the upper freshwater layer and lower brackish layer. At SWP3, floc sizes are observed to increase significantly in the depths near the saline mixing zone (lower 20% of the flow), with average floc sizes in the range of 100 to 600 μm (Fig. 3.6c). The same trend of an increase in floc size within the saline mixing zone is observed for both stations SWP4 and SWP5 (Fig. 3.6d and e). For both SWP4 and SWP5, average floc sizes range from around 100 μm to slightly less than 600 μm within the saline mixing layer. Example images of flocs observed within the saline mixing zone at SWP4 and SWP5 are presented in Figure 3.7. An increase in floc size is also present near the bed at station SWP4, likely consisting of flocs resuspended from the bed. Average floc sizes at SWP6 are relatively uniform both within the freshwater, saline mixing, and marine zones.

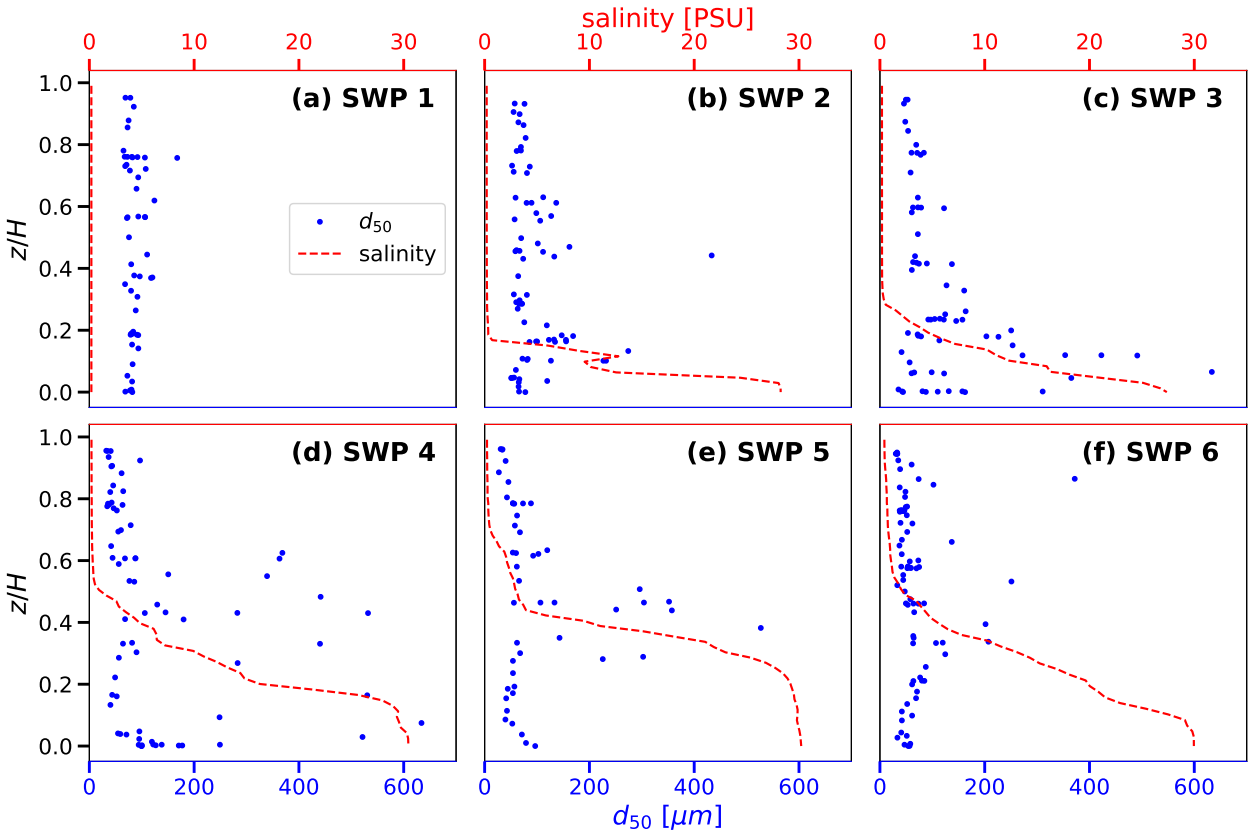

Figure 3.6: d_{50} floc size and salinity information collected at 6 stations along Southwest Pass during the winter survey while a salt wedge was in place. Data for Figures a - d were collected on January 9, 2021, and data for e and f were collected on January 12, 2021.

3.5.2 Floc settling velocity results

Rouse profile analysis

A Rouse profile was fit to the mud fraction of suspended sediment to investigate the bulk settling velocity of flocculated mud within three freshwater sections of the Mississippi River. The analysis was performed for SSC profiles collected at the BCS and VMC during both the summer and winter surveys. In addition, SWP1 from the winter survey is included in the analysis. Measured and calculated input parameters used for the analysis are presented in Table 3.2. In Table 3.2, values for the skin friction component of shear velocity were excluded for VMC and SWP1 during the winter survey since the bed consisted mainly of

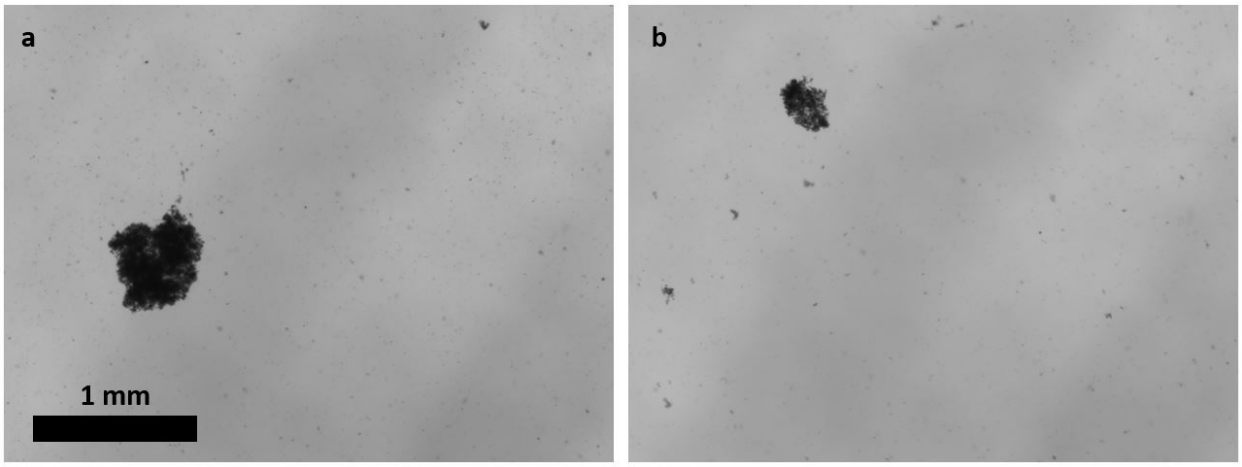

Figure 3.7: Example images of flocs collected within the stratified mixing layer at (a) SWP4 and (b) SWP5.

mud and no bedforms were observed during the survey.

Table 3.2: Measured (U, H, C_b) and calculated (u_*, u_{*s}, C_{5t}, α) input parameters used in the Rouse profile analysis. Water surface slope, S_0, was estimated from Nittrouer et al. (2011).

Station	U [m/s]	H [m]	u_* [m/s]	u_{*s} [m/s]	C_b [mg/L]	C_{5t}	S_0	α
BCS Summer	1.05	23	0.094	0.037	136	7.7E-05	1.5E-05	0.79
VMC Summer	0.76	18	0.063	0.026	122	6.2E-05	6E-06	0.64
BCS Winter	0.89	20.5	0.098	0.037	160	1.2E-04	2E-05	0.75
VMC Winter	0.79	18.5	0.050	–	268	1.0E-04	6E-06	0.63
SWP1 Winter	0.62	17	0.040	–	484	1.9E-04	6E-06	0.59

The results of fitting a Rouse profile to the mud fraction of SSC profiles for the stations included in the analysis are presented in Figure 3.8. During the summer survey, estimated settling velocities range from 0.41 mm/s at the BCS to 0.52 mm/s at the VMC location (Fig.3.8a and b).

At the BCS during the winter survey, the mud fraction of SSC was observed to be close to uniform over the water column as observed in Figure 3.8c. As a result, the estimated settling velocity is much lower compared to settling velocity estimates for the other stations. Down river at the VMC and SWP1 locations, a larger gradient in SSC is observed compared

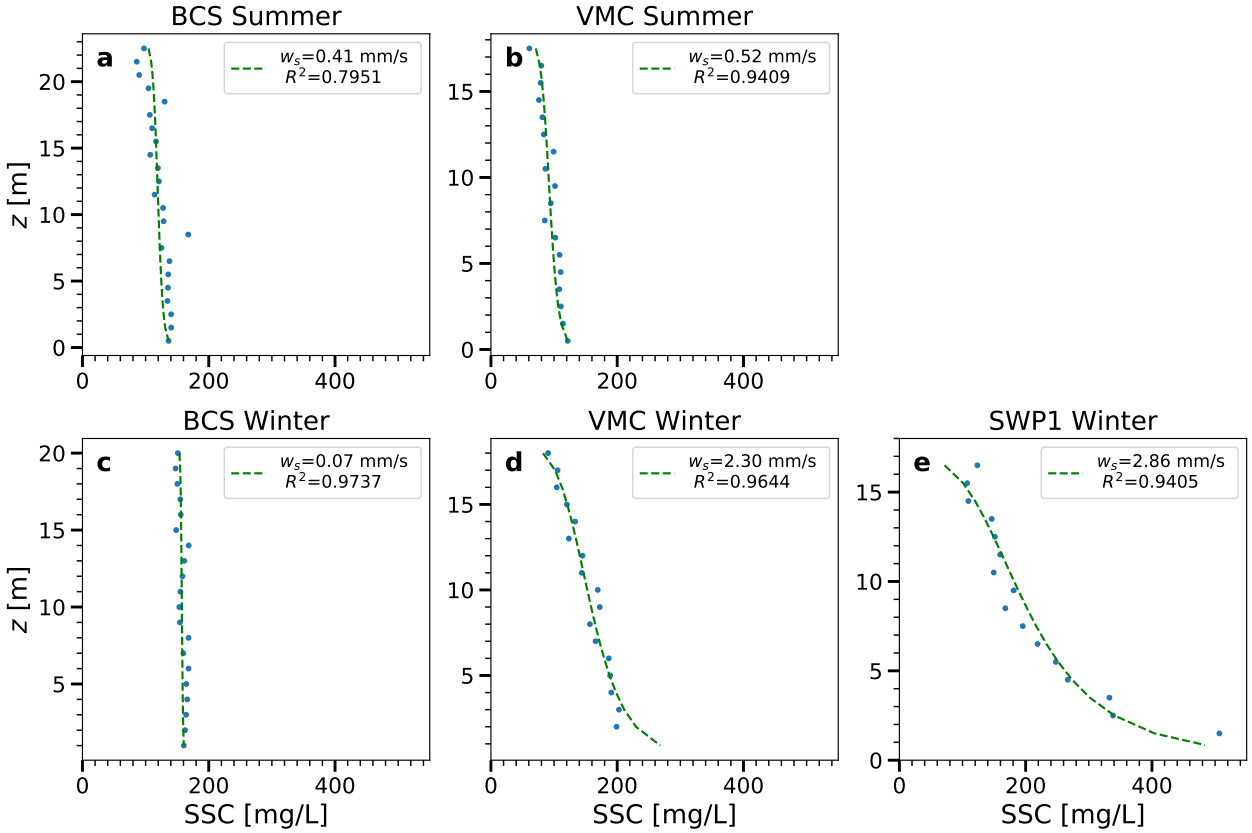

Figure 3.8: Mud fraction of SSC and fit Rouse profiles used to obtain an estimated bulk settling velocity.

to the other stations included in the analysis (Fig. 3.8d and e). Relatively high estimates of settling velocities of 2.30 mm/s and 2.86 mm/s are obtained for VMC and SWP1 during the winter, respectively. Possible explanations for these high settling velocity estimates, relative to the other stations, are considered in the Discussion.

Calculated values based on floc size

Settling velocity was also calculated using the measured floc sizes and equation 3.6. The following input values were used to make the calculations: the kinematic viscosity was taken as 0.89×10^{-6} and 1.47×10^{-6} m^2/s during the summer and winter, respectively to account for the difference in water temperature; The primary particle size, d_p was taken as 6.6 μm;

the submerged specific gravity of the particles, R_s was set to 1.65; and the coefficients b_1 and b_2 were taken as 100 and 0, respectively. A bulk, volume weighted settling velocity for the n number of flocs, with a volume, $\forall_{f,i}$, was calculated as: $w_s = \sum_{i=1}^{n} w_{s,i} \forall_{f,i} / \sum_{i=1}^{n} \forall_{f,i}$. The bulk settling velocity was calculated for the full set of flocs observed at a particular station. The fractal dimension of all flocs was assumed to be the same, and was adjusted to obtain a settling velocity close to the estimated settling velocity obtained from the Rouse profile analysis (Fig. 3.8).

For the BCS and VMC summer stations, a fractal dimension required to obtain bulk settling velocities similar to those obtained from the Rouse profile analysis was found to be 2.4, as shown in Table 3.3. Though, a fractal dimension of 2.4 results in an estimates settling velocity that is much smaller than the settling velocity estimated from the Rouse profile analysis for the winter survey locations.

Table 3.3: Settling velocities estimated from the Rouse profile analysis and using a floc settling velocity model (Eq. 3.6).

Station	w_s [mm/s]		
	Rouse Profile	$N_{f3} = 2.4$	$N_{f3} = 3.0$
BCS Summer	0.41	0.41	3.44
VMC Summer	0.52	0.53	5.16
BCS Winter	0.07	0.14	0.96
VMC Winter	2.30	0.19	1.54
SWP1 Winter	2.86	0.22	1.80

Just as the fractal dimension was adjusted to estimate a settling velocity with the model that closely matches the settling velocity obtained for the BCS and VMC data, the fractal dimension was adjusted to attempt to do the same for the winter survey stations. Under the input conditions for b_1 and b_2 that Strom and Keyvani (2011) obtained the best fit when developing the model, there is no suitable fractal dimension that provides an estimated settling velocity in the range of settling velocities estimated for VMC and SWP1 during the

winter survey. That is, since the input to the model provided from the data obtained at the BCS and VMC stations during the winter is floc size, flocs observed at these two stations are too small to achieve a settling velocity obtained from the model that is similar to those obtained from the Rouse profile analysis. Even with an unreasonably large fractal dimension of 3 (a solid), estimated settling velocities are nearly two thirds less than the Rouse profile estimated settling velocities.

Comparing the results of the Rouse profile analysis to settling velocity estimates from a floc settling velocity model show that under the constraints that the model was created, a bulk settling velocity similar to those observed from the Rouse profile analysis for the summer stations could be obtained with a reasonable fractal dimension input. However, the same result was not achievable for the VMC and SWP1 winter data.

3.6 Discussion

3.6.1 Observations of floc size over the water column

To the authors' best knowledge, this study presents the first direct in-situ observations of flocs within the Mississippi River. Galler and Allison (2008) investigated the possibility of mud flocculation within the lower Mississippi River by collecting water samples with Niskin bottles to perform settling column tests on board their research vessel during a survey in June 2003. The observed settling rates led Galler and Allison (2008) to estimate that a third of the sediment mass within the settling column consisted of flocs smaller than 110 μm, and another third of the mass consisted of flocs larger than 567 μm. This range of floc sizes is in the range of floc sizes observed directly in this study during the summer survey. Similar mean floc sizes, in the range of 43 to 181 μm were observed with a LISST-100x at 23 stations along 1532 km of the Yangtze River by Guo and He (2011).

This study confirms that flocs are present within the freshwater reaches of the Mississippi River during both the summer and winter. Differences in average floc sizes are present between the two seasons under similar discharge conditions, with flocs observed during the winter being smaller on average. Such a differences in average floc sizes could be attributed in part to differences in biological activity and makeup within the water as a result of an approximately 21 degrees Celsius difference in water temperature between the two seasons. Similar trends of floc size decreasing with depth is consistent between the two seasons. A possible explanation for this could be that floc sizes are adjusting depending on turbulence levels within the water column, with an increase in turbulence approaching the bed causing a reduction in floc sizes relative to further up in the water column.

The increase in floc size within the mixing zone between the upper freshwater and lower marine layer of the salt wedge within SWP is interesting and unexpected. A similar observation of an increase in floc size within the mixing zone of a vertical salinity stratified area of the Pearl River estuary was made by Zhang et al. (2021) with a LISST-200x. At one period of time throughout their study, flocs were observed to be uniform, around 10 μm in size within the freshwater and marine layer, but flocs within the mixing zone between the two layers were observed to range from 10 to just under 300 μm. This observation is in line with the observations made within SWP where d_{50} floc sizes were relatively uniform within the upper freshwater and lower marine layers. Though, d_{50} floc sizes of around 40 to 100 μm within the freshwater and marine layer were much larger in SWP compared to the 10 μm floc sizes observed by Zhang et al. (2021). Observations of SSC within the mixing layer also differed between the two locations. Zhang et al. (2021) observed SSC to increase close to linearly within the mixing layer to a close to uniform concentration that extended to the bed. SSC measurements within SWP were observed to decrease within the mixing layer relative to the upper freshwater layer, then transitioning back to increasing in concentration approaching the bed within the marine layer. Zhang et al. (2021) attribute the increase in floc

size within the mixing layer to be a result of the density stratification; however, no physical mechanism was proposed. A concern when sizing particles in-situ within a pycnocline is the possibility of influences from schlieren due to differences in density within the volume of fluid that sediment size is being measured (Mikkelsen et al., 2008). Mikkelsen et al. (2008) observed that both a LISST and a camera based particle sizing instrument falsely identified schlieren as particles within a pycnocline; though, schlieren within the images was visually apparent. All images collected within the pycnocline in SWP were visually observed for schlieren, though none was observed. The similar observations of an increase in floc size witin the pycnocline may suggests that an increase in floc size within the mixing layer could be a common phenomenon induced by similar biogeochemical or turbulence controls in the zone where fresh river water and saline marine water mix.

3.6.2 Floc settling velocity and mud SSC profiles

Flocculation of mud has the potential to increase the settling velocity of mud to much larger values compared to its unaggregated values. For example, the calculated settling velocities for the summer survey at the BCS and VMC range from 0.41 to 0.53 mm/s. These settling velocities correspond to an equivalent silt grain with a diameter between 20 to 23 μm. However, considering that the characteristic primary particle size that makes up the flocs is likely between 3 to 10 μm, the calculated settling velocities are anywhere from 4 to 58 times greater than the settling velocity of the characteristic primary particles. This also holds true for the VMC and SWP1 winter stations when considering the settling velocities estimated with the floc settling velocity model. The calculated settling velocities of 0.19 and 0.22 mm/s correspond to an equivalent silt grain between 17.5 to 19 μm.

If mud within a rivers is unflocculated, the unaggregated particles would be expected to be distributed close to uniformly over the water column as a result of their small settling

velocities. However, with flocculation having the potential to increase settling velocities to much larger values than that of the unaggregated particles, the presence of flocs can result in observable concentration gradients for the mud fraction of suspended sediment. Recently Lamb et al. (2020) analyzed disaggregated mud size and concentration profile data obtained from a range of lab and field measurements. They hypothesized that if flocculation of mud was present, this could be observed through vertical variations in mud concentration of individual grain-size classes. That is, vertical variations in concentration would be present for size classes that would be expected to be distributed uniformly over the water column if no flocculation was present. They tested this hypothesis by analyzing individual grain-size classes from the mud size and concentration data, from the multiple data sources, in a Rouse profile analysis to obtain effective settling velocities for each grain-size class. Their results indicated that mud effective settling velocities range from 0.17 to 0.70 mm/s, with a geometric mean of 0.34 mm/s. This range of settling rates is in agreement with the 0.19-0.53 mm/s settling velocity of mud calculated in this study from direct field observations of flocculated mud in the lowermost Mississippi River during the summer and winter. The large effective settling velocity of flocculated mud observed within the Mississippi River can explain observed vertical gradient in mud concentration.

3.6.3 VMC and SWP1 winter concentration profiles

Settling velocities estimated from the Rouse profile fit to the VMC and SWP1 winter concentration profiles appear to be high considering floc sizes were smaller in the winter compared to the summer. Though not proven, possible explanations for the high estimated settling velocities could include:(1) the assumption that form drag is insignificant is incorrect and should be accounted for in the shear velocity; (2) An influential amount of sand and coarse silt was in suspension and collected with water samples, increasing the sediment concentra-

tion near the bed; (3) The mud bed observed at VMC and SWP1 during the winter was net erosional as river discharge increased over the course of the survey, violating the Rouse profile assumption that erosion of the bed is in equilibrium with deposition and thereby resulting in higher near-bed concentrations than would be expected under equilibrium conditions. The assumption that the form drag component of shear velocity was negligible during the winter survey at VMC and SWP1 was made as a result of not observing large scale bedform contours from single-beam sonar images observed while on-board the research vessel. If the skin friction component of shear velocity at VMC and SWP1 during the winter was calculated with Equation 3.4, the values associated with the stations would decrease to 0.023 m/s and 0.018 m/s. Applying this decrease in shear velocity to the Rouse profile analysis reduces the estimated settling velocities to 1.07 and 1.32 mm/s for VMC and SWP1 during the winter survey — a nearly 54% decrease in estimated settling velocity at both stations. However, the estimated settling velocities are still somewhat high considering they correspond to an equivalent silt diameter of around 44 μm using Stokes' law assuming a density of sand. In contrast, the calculated settling velocities of 2.3 mm/s and 2.9 mm/s (derived from the Rouse profile analysis assuming form drag is negligible), correspond to an equivalent silica sphere of approximately 61.3 μm and 68.4 μm, respectively. Though if large silt and small sand was collected in the water samples, this has the potential to skew the SSC closer to the bed and increase the estimated settling velocity from the Rouse profile analysis as a result. For future surveys, the contribution of silt and sand to the total SSC can be accounted for by sizing disaggregated sediment samples before filtering.

An additional possible explanation for the high estimated settling velocity obtained from the VMC and SWP1 data during the winter could be a result of net erosion of the mud bed. If this is the case, the assumption that erosion of the bed is in equilibrium with deposition, made in deriving the Rouse profile equation, would be violated resulting in higher SSC near the bed. It was hypothesized that the mud bed at VMC and SWP1 observed during the

winter survey was deposited in the presence of a salt wedge that had migrated up river past these stations as a result of low river discharge proceeding the survey. In the week leading up to the survey, river discharge had increased significantly and presumably pushed the salt wedge out of the main channel. This increase in discharge could potentially produce a high enough bed shear stress to cause net erosion of the bed.

3.7 Conclusions

This study presents the first direct measurements of floc sizes within the freshwater reaches of the Mississippi River's main channel and the vertically stratified Southwest Pass distributary.

Within the main channel at the BCS and VMC during the summer survey, mean floc sizes were observed to range from 75 to 200 μm. Winter floc sizes ranged from 50 to 125 μm. Floc populations within the main channel were observed to be finer near the bed compared to further up in the water column. During the winter survey, flocs were observed within SWP in the presence of a salt wedge. The largest mean floc sizes, in the range of 100 to 600 μm, were observed within the mixing zone between the upper freshwater layer and the lower marine layer.

SSC profiles of the mud fraction of suspended sediment were used to estimate a bulk settling velocity for the floc and silt fraction of suspended sediment. For the most part, the observed floc sizes were large enough to produce sufficiently high settling velocities that could cause observed vertical mud concentration gradients.

Overall, the study highlights that the majority of the mud, in both summer and winter, in the freshwater reaches of the Mississippi River is flocculated. Floc sizes do not vary significantly in the freshwater portion of the river, but there is a tendency for flocs to be larger in the upper half of the water column. Flocs were also larger during summer (when SSC and temperature were both elevated) and in the mixing zone between the bottom marine

water and overlying fresh water; salinity in the mixing zone was elevated relative to fresh water with a likely decrease in turbulence.

While these measurements point to the importance of flocculation in controlling mud settling rates in the Mississippi River, they also highlight the need for additional in-situ observations. More data is needed to fully understand the role of the hydrodynamic, suspended sediment quantity and composition, organic material, and salts in controlling floc size and settling velocities within the fluvial environment.

Chapter 4

Conclusions

This thesis presents the development and use of a new in-situ particle sizing instrument that was designed to image flocs. The instrument and novel processing methods were developed and applied to particle data collected within the lowermost Mississippi River. Data collection on the lowermost Mississippi River focused on collecting floc size data at various locations along the river with differing hydrodynamic conditions. This data was then used to investigate the role of floc size on vertical concentration gradients of mud.

In Chapter 2, the development of the FlocARAZI is introduced. The FlocARAZI is a relatively inexpensive camera-based, in-situ microscope particle sizing instrument that can resolve particles down to 6 μm and has a field of view of 3.7 x 2.8 mm. Previously developed image processing methods, which were slightly modified, provide a means to obtain particle size data from the collected images. The output data from the image processing routing were used with a model for estimating the 3D fractal dimension of individual flocs. This floc size and 3D fractal dimension data was used to develop a method for estimating the mass concentration of flocculated suspended sediment from the obtained image data. The method can accurately estimate SSC for flocculated sediment concentrations up to 500 mg/L. In addition, texture and size characteristics of the imaged particles were used to train a machine learning SVM model that is accurate in distinguishing sand from flocs. This SVM model allows for obtaining in-situ particle size statistics for the flocculated mud fraction of suspended sediment separate from the full particle range size statistics. Part of the goal in designing the FlocARAZI was to make the instrument inexpensive and reproducible so

others can build their own unit to obtain in-situ observations of floc and suspended particle data to contribute to the cohesive sediment community. As such, the build instructions and image processing code will be publicly available.

In Chapter 3, the FLocARAZI and methods developed in Chapter 2 were used to obtain floc size and suspended sediment concentration profiles from floc data collected in the lowermost Mississippi River. Mean floc sizes were observed to range from 50 to 200 μm within the freshwater reaches of the river. On average, floc sizes observed during the winter were smaller than those observed during the summer at the same locations within the river. Both during the summer and the winter, fining of the flocculated sediment was observed near the bed relative to further up in the water column. The largest flocs were observed in the presence of a salt wedge within Southwest Pass. Flocs were observed to be relatively uniform, around 100 μm in size, both within the upper freshwater layer and the lower marine layer within the salt wedge. In contrast, average floc sizes within the mixing layer between the upper freshwater layer and lower marine layer were observed to range in size from 100 μm, up to 600 μm. In addition to observing floc sizes, the concentration data for the mud fraction of suspended sediment was used in a Rouse profile analysis to observe possible contributions of flocculation to the observed vertical concentration gradient. From the Rouse profile analysis, bulk settling velocity estimates from the summer for the mud fraction of suspended sediment ranged from around 0.4 to 0.5 mm/s. The results were tested against a floc settling velocity model, that produced similar settling velocities after assuming a reasonable fractal dimension for the model. Settling velocity estimates from the winter were anomalous and potential explanations were considered. Overall, this work provides new insight into floc size variations by season and location within the lowermost Mississippi River.

Bibliography

Agrawal, Y. C. and Pottsmith, H. C. (2000). Instruments for particle size and settling velocity observations in sediment transport. *Marine Geology*, 168(1):89–114.

Antonenkov, D. A. (2016). Method of the Aquatic Environment Image Processing for Determining the Mineral Suspension Parameters. *Physical Oceanography*, (5).

Bale, A. J. and Morris, A. W. (1987). In situ measurement of particle size in estuarine waters. *Estuarine, Coastal and Shelf Science*, 24(2):253–263.

Benson, T. and French, J. R. (2007). InSiPID: A new low-cost instrument for in situ particle size measurements in estuarine and coastal waters. *Journal of Sea Research*, 58(3):167–188.

Bird, E. C. F. (1996). Coastal Erosion and Rising Sea-Level. In Milliman, J. D. and Haq, B. U., editors, *Sea-Level Rise and Coastal Subsidence: Causes, Consequences, and Strategies*, Coastal Systems and Continental Margins, pages 87–103. Springer Netherlands, Dordrecht.

Bowers, D. G., McKee, D., Jago, C. F., and Nimmo-Smith, W. A. M. (2017). The area-to-mass ratio and fractal dimension of marine flocs. *Estuarine, Coastal and Shelf Science*, 189:224–234.

Cartwright, G. M., Friedrichs, C. T., and Sanford, L. P. (2011). In situ characterization of estuarine suspended sediment in the presence of muddy flocs and pellets. In *The Proceedings of the Coastal Sediments 2011*, pages 642–655. World Scientific Publishing Company.

Colten, C. E. (2018). Levees and the Making of a Dysfunctional Floodplain. In Day, J. W.

and Erdman, J. A., editors, *Mississippi Delta Restoration: Pathways to a sustainable future*, Estuaries of the World, pages 29–37. Springer International Publishing, Cham.

Davies, E. J. and Nepstad, R. (2017). In situ characterisation of complex suspended particulates surrounding an active submarine tailings placement site in a Norwegian fjord. *Regional Studies in Marine Science*, 16:198–207.

Davies, E. J., Nimmo-Smith, W. A. M., Agrawal, Y. C., and Souza, A. J. (2012). LISST-100 response to large particles. *Marine Geology*, 307-310:117–122.

Day, J. W., Christian, R. R., Boesch, D. M., Yáñez-Arancibia, A., Morris, J., Twilley, R. R., Naylor, L., Schaffner, L., and Stevenson, C. (2008). Consequences of Climate Change on the Ecogeomorphology of Coastal Wetlands. *Estuaries and Coasts*, 31(3):477–491.

Dyer, K. R., Cornelisse, J., Dearnaley, M. P., Fennessy, M. J., Jones, S. E., Kappenberg, J., McCave, I. N., Pejrup, M., Puls, W., Van Leussen, W., and Wolfstein, K. (1996). A comparison of in situ techniques for estuarine floc settling velocity measurements. *Journal of Sea Research*, 36(1):15–29.

Dyer, K. R. and Manning, A. J. (1999). Observation of the size, settling velocity and effective density of flocs, and their fractal dimensions. *Journal of Sea Research*, 41(1):87–95.

Einstein, H. A. and Krone, R. B. (1962). Experiments to determine modes of cohesive sediment transport in salt water. *Journal of Geophysical Research (1896-1977)*, 67(4):1451–1461.

Eisma, D. (1986). Flocculation and de-flocculation of suspended matter in estuaries. *Netherlands Journal of Sea Research*, 20(2):183 – 199.

Emanuel, K. (2005). Increasing destructiveness of tropical cyclones over the past 30 years. *Nature*, 436(7051):686–688.

Esposito, C. R., Shen, Z., Törnqvist, T. E., Marshak, J., and White, C. (2017). Efficient retention of mud drives land building on the Mississippi Delta plain. *Earth Surface Dynamics*, 5(3):387–397.

Fall, K. A., Friedrichs, C. T., Massey, G. M., Bowers, D. G., and Smith, S. J. (2021). The Importance of Organic Content to Fractal Floc Properties in Estuarine Surface Waters: Insights From Video, LISST, and Pump Sampling. *Journal of Geophysical Research: Oceans*, 126(1):e2020JC016787.

Felix, D., Albayrak, I., and Boes, R. M. (2013). Laboratory investigation on measuring suspended sediment by portable laser diffractometer (LISST) focusing on particle shape. *Geo-Marine Letters*, 33(6):485–498.

Fennessy, M. J., Dyer, K. R., and Huntley, D. A. (1994). inssev: An instrument to measure the size and settling velocity of flocs in situ. *Marine Geology*, 117(1):107 – 117.

Ferguson, R. I. and Church, M. (2004). A Simple Universal Equation for Grain Settling Velocity. *Journal of Sedimentary Research*, 74(6):933–937.

Filippa, L., Freire, L., Trento, A., Álvarez, A. M., Gallo, M., and Vinzón, S. (2011). Laboratory evaluation of two LISST-25X using river sediments. *Sedimentary Geology*, 238(3):268–276.

Flesch, J. C., Spicer, P. T., and Pratsinis, S. E. (1999). Laminar and turbulent shear-induced flocculation of fractal aggregates. *AIChE Journal*, 45(5):1114–1124.

Fox, J. M., Hill, P. S., Milligan, T. G., and Boldrin, A. (2004). Flocculation and sedimentation on the Po River Delta. *Marine Geology*, 203(1):95–107.

Galler, J. J. and Allison, M. A. (2008). Estuarine controls on fine-grained sediment storage in the Lower Mississippi and Atchafalaya Rivers. *GSA Bulletin*, 120(3-4):386–398.

González, J. L. and Tornqvist, T. E. (2006). Coastal Louisiana in crisis: Subsidence or sea level rise? *Eos, Transactions American Geophysical Union*, 87(45):493–498.

Graham, G. W., Davies, E. J., Nimmo-Smith, W. a. M., Bowers, D. G., and Braithwaite, K. M. (2012). Interpreting LISST-100X measurements of particles with complex shape using digital in-line holography. *Journal of Geophysical Research: Oceans*, 117(C5).

Guo, C., He, Q., Guo, L., and Winterwerp, J. C. (2017). A study of in-situ sediment flocculation in the turbidity maxima of the Yangtze Estuary. *Estuarine, Coastal and Shelf Science*, 191:1–9.

Guo, L. and He, Q. (2011). Freshwater flocculation of suspended sediments in the Yangtze River, China. *Ocean Dynamics*, 61(2/3):371–386.

Hill, P. S., Boss, E., Newgard, J. P., Law, B. A., and Milligan, T. G. (2011). Observations of the sensitivity of beam attenuation to particle size in a coastal bottom boundary layer. *Journal of Geophysical Research: Oceans*, 116(C2).

Hill, P. S., Syvitski, J. P., Cowan, E. A., and Powell, R. D. (1998). In situ observations of floc settling velocities in Glacier Bay, Alaska. *Marine Geology*, 145(1):85–94.

Karageorgis, A., Georgopoulos, D., Gardner, W., Mikkelsen, O., and Velaoras, D. (2015). How schlieren affects beam transmissometers and LISST-Deep: an example from the stratified Danube River delta, NW Black Sea. *Mediterranean Marine Science*, 16(2):366–372.

Karp-Boss, L., Azevedo, L., and Boss, E. (2007). LISST-100 measurements of phytoplankton size distribution: evaluation of the effects of cell shape. *Limnology and Oceanography: Methods*, 5(11):396–406.

Kenney, M. A., Hobbs, B. F., Mohrig, D., Huang, H., Nittrouer, J. A., Kim, W., and Parker,

G. (2013). Cost analysis of water and sediment diversions to optimize land building in the Mississippi River delta. *Water Resources Research*, 49(6):3388–3405.

Kennish, M. J. (2002). Environmental threats and environmental future of estuaries. *Environmental Conservation*, 29(1):78–107.

Keyvani, A. and Strom, K. (2013). A fully-automated image processing technique to improve measurement of suspended particles and flocs by removing out-of-focus objects. *Computers & Geosciences*, 52:189–198.

Kim, W., Mohrig, D., Twilley, R., Paola, C., and Parker, G. (2009). Is It Feasible to Build New Land in the Mississippi River Delta? *Eos, Transactions American Geophysical Union*, 90(42):373–374.

Krone, R. B. (1962). *Flume studies of the transport of sediment in estuarial shoaling processes; final report*. Hydraulic Engineering Laboratory and Sanitary Engineering Research Laboratory, University of California, Berkeley.

Kulp, S. A. and Strauss, B. H. (2019). New elevation data triple estimates of global vulnerability to sea-level rise and coastal flooding. *Nature Communications*, 10(1):4844.

Kumar, R. G., Strom, K. B., and Keyvani, A. (2010). Floc properties and settling velocity of San Jacinto estuary mud under variable shear and salinity conditions. *Continental Shelf Research*, 30(20):2067–2081.

Lamb, M. P., de Leeuw, J., Fischer, W. W., Moodie, A. J., Venditti, J. G., Nittrouer, J. A., Haught, D., and Parker, G. (2020). Mud in rivers transported as flocculated and suspended bed material. *Nature Geoscience*, 13(8):566–570.

Li, D. H. and Ganczarczyk, J. (1989). Fractal geometry of particle aggregates generated

in water and wastewater treatment processes. *Environmental Science & Technology*, 23(11):1385–1389.

MacDonald, I. T. and Mullarney, J. C. (2015). A Novel "FlocDrifter" Platform for Observing Flocculation and Turbulence Processes in a Lagrangian Frame of Reference. *Journal of Atmospheric and Oceanic Technology*, 32(3):547–561.

Maggi, F., Mietta, F., and Winterwerp, J. C. (2007). Effect of variable fractal dimension on the floc size distribution of suspended cohesive sediment. *Journal of Hydrology*, 343(1):43–55.

Maggi, F. and Winterwerp, J. C. (2004). Method for computing the three-dimensional capacity dimension from two-dimensional projections of fractal aggregates. *Physical Review E*, 69(1):011405.

Manning, A. J., Bass, S. J., and Dyer, K. R. (2006). Floc properties in the turbidity maximum of a mesotidal estuary during neap and spring tidal conditions. *Marine Geology*, 235(1):193–211.

Manning, A. J. and Dyer, K. R. (2002). The use of optics for the in situ determination of flocculated mud characteristics. *Journal of Optics A: Pure and Applied Optics*, 4(4):S71–S81.

McGranahan, G., Balk, D., and Anderson, B. (2007). The rising tide: assessing the risks of climate change and human settlements in low elevation coastal zones. *Environment and Urbanization*, 19(1):17–37.

Mie, G. (1908). Beiträge zur Optik trüber Medien, speziell kolloidaler Metallösungen. *Annalen der Physik*, 330(3):377–445.

Mietta, F., Chassagne, C., and Winterwerp, J. C. (2009). Shear-induced flocculation of a suspension of kaolinite as function of pH and salt concentration. *Journal of Colloid and Interface Science*, 336(1):134–141.

Mikkelsen, O. A., Hill, P. S., and Milligan, T. G. (2006). Single-grain, microfloc and macrofloc volume variations observed with a LISST-100 and a digital floc camera. *Journal of Sea Research*, 55(2):87–102.

Mikkelsen, O. A., Hill, P. S., and Milligan, T. G. (2007). Seasonal and spatial variation of floc size, settling velocity, and density on the inner Adriatic Shelf (Italy). *Continental Shelf Research*, 27(3):417–430.

Mikkelsen, O. A., Hill, P. S., Milligan, T. G., and Chant, R. J. (2005). In situ particle size distributions and volume concentrations from a LISST-100 laser particle sizer and a digital floc camera. *Continental Shelf Research*, 25(16):1959–1978.

Mikkelsen, O. A., Milligan, T. G., Hill, P. S., Chant, R. J., Jago, C. F., Jones, S. E., Krivtsov, V., and Mitchelson-Jacob, G. (2008). The influence of schlieren on in situ optical measurements used for particle characterization. *Limnology and Oceanography: Methods*, 6(3):133–143.

Milligan, T. G. and Hill, P. S. (1998). A laboratory assessment of the relative importance of turbulence, particle composition, and concentration in limiting maximal floc size and settling behaviour. *Journal of Sea Research*, 39(3):227–241.

Morton, R. A. (2003). An Overview of Coastal Land Loss:With Emphasis on the Southeastern United States. *U.S. Geological Survey Open File Report*.

Möller, I., Kudella, M., Rupprecht, F., Spencer, T., Paul, M., van Wesenbeeck, B. K., Wolters, G., Jensen, K., Bouma, T. J., Miranda-Lange, M., and Schimmels, S. (2014).

Wave attenuation over coastal salt marshes under storm surge conditions. *Nature Geoscience*, 7(10):727–731.

Nittrouer, J. A., Best, J. L., Brantley, C., Cash, R. W., Czapiga, M., Kumar, P., and Parker, G. (2012). Mitigating land loss in coastal Louisiana by controlled diversion of Mississippi River sand. *Nature Geoscience*, 5(8):534–537.

Nittrouer, J. A., Mohrig, D., and Allison, M. (2011). Punctuated sand transport in the lowermost Mississippi River. *Journal of Geophysical Research: Earth Surface*, 116(F4).

Noble, W. S. (2006). What is a support vector machine? *Nature Biotechnology*, 24(12):1565–1567.

Nordenson, C. S., Nordenson, G., and Chapman, J. (2018). Structures of Coastal Resilience. In Nordenson, C. S., Nordenson, G., and Chapman, J., editors, *Structures of Coastal Resilience*, pages 73–122. Island Press/Center for Resource Economics, Washington, DC.

Osborn, R., Dillon, B., Tran, D., Abolfazli, E., Dunne, K. B. J., Nittrouer, J. A., and Strom, K. (2021). FlocARAZI: An in-situ image-based particle sizing instrument capable of estimating SSC and distinguishing sand from flocs. *Submitted for review in Journal of Geophysical Research: Earth Surface*.

Osborn, R., Dunne, K. B. J., Abolfazli, E., Strom, K., and Nittrouer, J. A. (2020). Characterization of In-Situ Floc Sizes Over the Vertical Within the Mississippi River and its Distributaries. AGU.

Potter, P. E., Maynard, J., and Depetris, P. J. (2005). *Mud and mudstones : introduction and overview*. Springer.

Rasband, W. S. (2012). ImageJ: Image processing and analysis in Java. *Astrophysics Source Code Library*, page ascl:1206.013.

Rouse, H. (1939). An Analysis of Sediment Transportation in the Light of Fluid Turbulence. Conference Name: Annual Meeting of the American Society of Civil Engineers Meeting Name: Annual Meeting of the American Society of Civil Engineers Num Pages: 40 Place: Washington, DC Publisher: United States Department of Agriculture.

Schieber, J., Southard, J. B., Kissling, P., Rossman, B., and Ginsburg, R. (2013). Experimental Deposition of Carbonate Mud From Moving Suspensions: Importance of Flocculation and Implications For Modern and Ancient Carbonate Mud DepositionCurrent Ripples. *Journal of Sedimentary Research*, 83(11):1026–1032.

Sheng, Y. P., Lapetina, A., and Ma, G. (2012). The reduction of storm surge by vegetation canopies: Three-dimensional simulations. *Geophysical Research Letters*, 39(20).

Smith, S. J. and Friedrichs, C. T. (2011). Size and settling velocities of cohesive flocs and suspended sediment aggregates in a trailing suction hopper dredge plume. *Continental Shelf Research*, 31(10, Supplement):S50–S63.

Smith, S. J. and Friedrichs, C. T. (2015). Image processing methods for in situ estimation of cohesive sediment floc size, settling velocity, and density. *Limnology and Oceanography: Methods*, 13(5):250–264.

Strom, K. and Keyvani, A. (2011). An Explicit Full-Range Settling Velocity Equation for Mud Flocs. *Journal of Sedimentary Research*, 81(12):921–934.

Tran, D., Kuprenas, R., and Strom, K. (2018). How do changes in suspended sediment concentration alone influence the size of mud flocs under steady turbulent shearing? *Continental Shelf Research*, 158:1–14.

Walling, D. E. and Fang, D. (2003). Recent trends in the suspended sediment loads of the world's rivers. *Global and Planetary Change*, 39(1):111–126.

Winterwerp, J. C., Manning, A. J., Martens, C., de Mulder, T., and Vanlede, J. (2006). A heuristic formula for turbulence-induced flocculation of cohesive sediment. *Estuarine, Coastal and Shelf Science*, 68(1):195–207.

Wright, S. and Parker, G. (2004a). Density Stratification Effects in Sand-Bed Rivers. *Journal of Hydraulic Engineering*, 130(8):783–795.

Wright, S. and Parker, G. (2004b). Flow Resistance and Suspended Load in Sand-Bed Rivers: Simplified Stratification Model. *Journal of Hydraulic Engineering*, 130(8):796–805.

Xu, K., Bentley, S. J., Day, J. W., and Freeman, A. M. (2019). A review of sediment diversion in the Mississippi River Deltaic Plain. *Estuarine, Coastal and Shelf Science*, 225:106241.

Zack, G. W., Rogers, W. E., and Latt, S. A. (1977). Automatic measurement of sister chromatid exchange frequency. *Journal of Histochemistry & Cytochemistry*, 25(7):741–753.

Zhang, Y., Ren, J., Zhang, W., and Wu, J. (2021). Importance of salinity-induced stratification on flocculation in tidal estuaries. *Journal of Hydrology*, page 126063.

Zhu, Z., Yu, J., Wang, H., Dou, J., and Wang, C. (2015). Fractal Dimension of Cohesive Sediment Flocs at Steady State under Seven Shear Flow Conditions. *Water*, 7(8):4385–4408.